University of Massachusetts Amherst
ScholarWorks@UMass Amherst

Doctoral Dissertations 1896 - February 2014

1-1-1977

The nature of the circumstellar envelopes of MR 119 and P Cygni.

William Randolph Oegerle
University of Massachusetts Amherst

Follow this and additional works at: https://scholarworks.umass.edu/dissertations_1

Recommended Citation

Oegerle, William Randolph, "The nature of the circumstellar envelopes of MR 119 and P Cygni." (1977). *Doctoral Dissertations 1896 - February 2014*. 1730.
https://scholarworks.umass.edu/dissertations_1/1730

This Open Access Dissertation is brought to you for free and open access by ScholarWorks@UMass Amherst. It has been accepted for inclusion in Doctoral Dissertations 1896 - February 2014 by an authorized administrator of ScholarWorks@UMass Amherst. For more information, please contact scholarworks@library.umass.edu.

3 1206 6 0015 4643 8

THE NATURE OF THE CIRCUMSTELLAR ENVELOPES OF MR 119 AND P CYGNI

A Dissertation Presented

By

William Randolph Oegerle

Submitted to the Graduate School of the
University of Massachusetts in partial fulfillment
of the requirements for the degree of

DOCTOR OF PHILOSOPHY

April 1977

Astronomy

THE NATURE OF THE CIRCUMSTELLAR ENVELOPES OF MR 119 AND P CYGNI

A Dissertation Presented

By

William Randolph Oegerle

Approved as to style and content by:

David Van Blerkom

David J. Van Blerkom, Chairman of Committee

William M. Irvine, Member

Nicholas Z. Scoville, Member

Edward S. Chang

Edward S. Chang, Member

F W Byron J.

Frederick W. Byron, Jr., Head
Department of Physics and Astronomy

April 1977

ACKNOWLEDGEMENTS

The number of people who contributed to the completion of this work is truly astronomical. First, and foremost, I would like to thank my advisor, David Van Blerkom, for his patience, encouragement, and direction.

I also extend thanks to David Van Blerkom and Bill Irvine for financial support during part of my graduate career. The following list of fellow students and faculty helped make my graduate years less painful: Al Walstad, Paul Guthrie, John Sloan, Larry Esposito, Robin Waldron, Dave Harding, Lee Fowler, Dave Helfand, John Donoghue, Jeremy Wise, Tom Arny, and Gene Tademaru. The efficient and cheerful typing of this thesis by Nellie Bristol is gratefully acknowledged.

I am also indebted to my wife, Robin, for her patience and support during these years. I deeply appreciate the sacrifices she has made for the sake of my career.

Finally, I wish to thank my Mom and Dad, who instilled in me the desire to learn.

ABSTRACT

The Nature of the Circumstellar Envelopes of MR 119 and P Cygni

(May 1977)

William R. Oegerle, B.S., University of Florida
Ph.D., University of Massachusetts

Directed by: Professor David Van Blerkom

The physical conditions in the envelopes of P Cygni and MR 119, a representative WN8 star, are investigated using available observations of the HI, HeI, and infrared spectra. The general approach is to construct models of the envelopes by computing line intensities and profiles for various parameters such as the stellar temperature, mass loss rate, and the velocity of the outflow. Comparison of these models with the observations hopefully singles out a unique set of parameters.

A model for HeI emission in Wolf-Rayet envelopes is constructed and then compared with MR 119. At one point in the envelope, the non-LTE populations of the levels are computed by solving the statistical equilibrium equations using the escape probability method. Assuming homogeneity in the envelope, the line intensities are then calculated and compared with observations. The best fitting model indicates a mass loss rate of $\sim 10^{-4}\ M_{\odot}yr^{-1}$ and an envelope temperature of $\sim$ 20,000 K.

Recent work on the interpretation of hydrogen emission lines from P Cygni has led to contradictory models of its atmosphere. In order to resolve the problem, a model for HeI emission in an accelerating envelope was constructed. The resulting line profiles agree quite well with the observed lines for a mass loss rate of $2 \times 10^{-6}\ M_{\odot}yr^{-1}$. The

unusual behavior of the helium lines, in which absorption components of lines in the same series have quite different displacements from line center, is a natural consequence of the model. Recent observations of the infrared continuum indicate that the flow is accelerating more slowly than previously thought. Therefore, a model for the envelope, in which the velocity of the outflow increases linearly with radius, was constructed in order to produce the observed Balmer lines. Using a stellar temperature of 20,000 K and a mass loss rate of 1.5×10^{-5} $M_{\odot} yr^{-1}$, the computed Balmer lines were in fair agreement with the observed lines. Unfortunately, the model does not allow the formation of an arbitrarily deep absorption component. Therefore, the absorption components of the calculated profiles are much shallower than observed.

The Balmer lines observed in the spectrum of P Cygni are hard to produce in an accelerating flow because the central intensities of the emission peaks are very large, while the absorption features are very deep. It is shown that the only way to produce both of these features is to have the source function in the line decrease very rapidly with radius. The radial dependence of the source function for Hα is derived analytically, using a three level atom, and it is found that the source function can decrease rapidly at large radii.

Portions of this work have been published in the Astrophysical Journal. The model for MR 119 was published in Volume 206, page 150, and the model for the HeI lines in P Cygni appeared in Volume 208, page 453.

TABLE OF CONTENTS

		Page
Chapter I:	Introduction	1
	Circumstellar Envelopes	1
	Wolf-Rayet Stars	2
	P Cygni	4
Chapter II:	The Escape Probability Method	6
	Basic Concepts	6
	Constant Velocity Surfaces	7
	Line Profiles	8
	Features of Other Velocity Laws	9
Chapter III:	Wolf-Rayet Stars	14
	A One Point Model for MR 119	14
Chapter IV:	P Cygni	28
	Previous Observations and Interpretations	28
	A Model for the HeI Spectrum	30
	The Double Absorption Features	40
	The Early Balmer Lines	49
	Discussion of Results	63
Chapter V:	Summary	66
Appendix		71

LIST OF TABLES

Page

Table I. Singlet and triplet line intensities calculated by using a "one point model" for the Wolf-Rayet star MR 119 22

Table II. Equivalent widths of the absorption components for some singlet and triplet lines observed in the spectrum of P Cygni 39

FIGURE CAPTIONS

Page

Figure 1. Constant line of sight velocity surfaces for the velocity law $v = v_\infty (1 - R_*/r)^{1/2}$ . . . 8

Figure 2a. Constant line of sight velocity surfaces for the velocity law $v = v_o r/R_*$ 12

Figure 2b. Constant line of sight velocity surfaces for the decelerating velocity law $v = v_{max}(R_*/r)^{1/2}$ 12

Figure 3. Term diagram for HeI 16

Figure 4. The logarithm of the departure coefficient, $b_{n\ell}$, is plotted against the principal quantum number, n 23

Figure 5. The intensity of the transitions $n^3D - 2^3P$ relative to the intensity of the transition $4^3D - 2^3P$ is plotted as a function of n $(4 \leq n \leq 8)$ 25

Figure 6. Line profile for λ4387 32

Figure 7. Line profile for λ4026 33

Figure 8. Line profile for λ4471 34

Figure 9. Logarithm of the optical depths in the three lines λλ4471, 4387, and 4026 plotted against the distance from the star 37

Figure 10. The observed line profile of Balmer 10 . . . 41

Figure 11. Constant line of sight velocity surfaces for a flow that accelerates and then decelerates 45

Figure 12. Theoretical line profiles for Balmer 10 . . . 48

Figure 13. Line profiles for Hα 59

Figure 14. Line profiles for Hβ 60

Figure 15. Line profiles for Hγ 61

CHAPTER I

INTRODUCTION

Circumstellar Envelopes

Rocket observations of far ultraviolet stellar spectra have provided evidence of high velocity mass loss from hot supergiants. Absorption lines of the resonance transitions of CIV, NV, and SiIV have blue shifts corresponding to Doppler velocities in the 1000 - 2000 km s^{-1} range (Morton 1967). It is now generally accepted that the phenomenon of high velocity mass loss occurs in almost all hot supergiants and in a few giants of spectral type B0.5 and earlier (Morton 1968).

Wolf-Rayet and P Cygni stars have long been recognized as prominent members of the class of stars which lose mass. The spectra of both of these classes of stars are characterized by spectral lines with a nearly undisplaced emission component and a shortward displaced absorption component (in the case of P Cygni there may be double or even triple absorption components). The formation of this type of line profile, called a "P Cygni" profile, has long been explained by emission in a spherically expanding envelope surrounding the star (Beals 1929). Using this concept, it is possible to construct an emission model for a star undergoing mass loss. The profile of a line formed in the outflowing envelope will depend on the temperature and velocity distributions of the gas and the star's temperature and mass loss rate.

The purpose of this work is to determine the physical nature of the envelopes surrounding MR 119 (a typical late-type Wolf-Rayet star) and P Cygni. The HeII spectra in WN5 and WN6 stars have been investigated by Castor and Van Blerkom (1970), and a model for the early Balmer lines of P Cygni has been constructed by Kuan and Kuhi (1975). Since the ionization potential of HeI is substantially different from that of HeII and HI, the neutral helium lines would most likely be formed in a different region of the atmosphere. Therefore, an emission model based on the HeI lines would serve to give a more complete picture of the physical conditions in the envelope.

Wolf-Rayet Stars

There are three types of Wolf-Rayet (WR) stars known: the nuclei of some planetary nebulae, components of binary systems, and single Population I objects (Paczynski 1972). WR stars are classified as either WN or WC depending on whether the spectra are characterized by emission lines of He and N or He, C, and O respectively (Beals 1938). In this manuscript, we will be concerned only with the single Population I WN stars.

The WN stars are further subdivided into classes WN3 through WN8. Generally speaking, stars on the upper end of this sequence (i.e. WN7-8) have larger ratios of hydrogen to helium in their atmospheres and lower effective stellar temperatures than those on the lower end (Smith 1972). The single Population I objects typically have temperatures of 30,000 K, masses of 10 $M_\odot$, and luminosities of 2 x 10^5 $L_\odot$. Therefore, these stars are too luminous to be on the hydrogen main sequence and are thought to be in a "post main sequence" phase (Paczynski 1972). The observed outflow velocities in WR stars, as deduced from the doppler widths of the emission lines, are ∿ 1000 km s^{-1} implying that the mass loss rates are

$10^{-6} - 10^{-4}\ M_{\odot} yr^{-1}$.

There have been a number of mechanisms presented to explain the high mass loss rates in WR stars. A brief review of these suggestions will be given here because the velocity distribution in the envelope will depend on the mechanism causing the outflow.

Paczynski (1969) and Simon and Stothers (1960) have postulated that WR stars are vibrationally unstable because of the temperature sensitivity of the triple alpha reaction. In this model, mass loss would occur if the amplitude of the oscillation was large enough. Limber (1964) has suggested that a "forced rotation instability" could give rise to the mass loss. This model cannot explain the violet displaced absorption features seen in some emission lines. Rublev (1964) has proposed that radiation pressure in the continuum is responsible for the mass loss. It is true that the luminosities of WR stars are close to the Eddington limit (to be defined in the next section), but it seems that a stable interior solution cannot be built if the surface luminosity exceeds this limit.

Lucy and Solomon (1970) found that radiation pressure in resonance lines could lead to outflow velocities of ~ 1000 km s^{-1}. However, the maximum mass loss rate allowed by the mechanism is $L/c^2 \approx 10^{-8}\ M_{\odot} yr^{-1}$, which is several orders of magnitude too low. Castor, Abbott, and Klein (1975) have included the radiation pressure due to many subordinate lines of CIII in Of star envelopes and found that the maximum loss rate is $L/cv_{\infty} \approx 100\ L/c^2$. Therefore, radiation pressure in the lines appears to be a very promising mechanism for causing mass loss from early-type stars.

P Cygni

Although it is the prototype of a class of emission line stars, P Cygni (HD 193237) is unlike other members of its class in a number of respects. For one, P Cygni displays the classic "P Cygni" profile more completely than other members of the class. Second, P Cygni underwent a nova-like outburst in the year 1600. The outburst was very unusual, because the maximum brightness lasted for six years.

Because of its high apparent brightness, P Cygni has been observed in some detail (Adams and Merrill 1957, Beals 1950, de Groot 1969 and references therein) and lends itself to theoretical investigations of its excitation conditions and velocity distribution in the circumstellar envelope. The spectrum of P Cygni is very rich and includes many lines of hydrogen and neutral helium.

The most recent studies of P Cygni are those of de Groot (1969) and Kuan and Kuhi (1975), which reach quite different conclusions. By analyzing the Balmer lines, de Groot concluded that the outflow is accelerating, while Kuan and Kuhi analyzed the same lines and showed that a decelerating flow could produce the lines.

In 1967, Magalashvili and Kharadze reported that P Cygni's brightness varied with a period of .5006 days. This has never been verified, but the possibility is very interesting because P Cygni may be pulsationally unstable. If P Cygni conforms to the mass-luminosity relationship, then its visual absolute magnitude of -8 indicates a mass of $\sim 100\ M_{\odot}$. Schwarzschild and Härm (1959) have shown that any star more massive than $65\ M_{\odot}$ will be pulsationally unstable. Therefore, P Cygni could be losing mass through large amplitude pulsations. This type of mass loss could easily lead to shells in the ejected envelope and a decelerating flow.

On the other hand, radiation pressure must play an important role because P Cygni's luminosity is very close to the Eddington limit. This limit is defined as the luminosity for which the radiation force due to electron scattering balances the gravitational force of the star and can be written in the form

$$L_{edd} = 1.3 \times 10^{38} (M_*/M_\odot) \text{ ergs}^{-1} \quad . \tag{1}$$

Assuming a mass of 60 $M_\odot$ for P Cygni gives $L_{edd} \sim 2 \times 10^6 L_\odot$. Making the gross assumption that P Cygni radiates like a blackbody at a temperature of 20,000 K and has a radius of 90 $R_\odot$ (Barlow and Cohen 1977), the luminosity is $L = 4\pi R_*^2 \sigma T_*^4 \approx 1.5 \times 10^6 L_\odot$. Therefore, the luminosity of P Cygni is very close to the Eddington limit, indicating that radiation pressure may be the dominant mass loss mechanism. As shown by Castor, Abbott, and Klein (1975), radiation pressure leads to an accelerating outflow of gas.

The question of whether the outflow is accelerating or decelerating is an important one and will be addressed in Chapter IV.

CHAPTER II

THE ESCAPE PROBABILITY METHOD

Basic Concepts

The usual assumptions that are made in calculating model atmospheres for hot main sequence stars (hydrostatic equilibrium, radiative equilibrium, local thermodynamic equilibrium (LTE), and negligible curvature effects) are probably all violated in Wolf-Rayet and P Cygni stars (Van Blerkom 1972). The escape probability method developed by Sololev (1960) and extended by Castor (1970) has been employed with fair success in studies of Wolf-Rayet stars, novae, molecular clouds, and will also be used in this investigation.

The escape probability method can be used with a fair degree of confidence when the bulk velocity of the flow is much greater than the thermal velocity of the gas at the local electron temperature. In Wolf-Rayet stars, the maximum velocity of the gas in the envelope is 50-100 times larger than the thermal velocity, while for P Cygni this value is $\sim$ 20-30.

Consider a point in an expanding envelope surrounding a star. If there is a velocity gradient in the gas, a photon emitted at this point will be preferentially absorbed near its point of emission, or it will escape from the envelope because of the Doppler effect. Therefore, a transfer problem exists only in a narrow zone where the photon has a chance of being absorbed. The width of this zone is usually on the order of a few thermal Doppler widths.

Constant Velocity Surfaces

In order to illustrate how the escape probability method works, consider a velocity distribution in the envelope of the form

$$v(r) = v_\infty(1 - R_*/r)^{1/2} \quad , \tag{2}$$

which can be produced by radiation pressure acting on the gas (see Chapter III). We will also adopt the geometry of the envelope used by Castor (1970). The origin of the Cartesian coordinate system is centered on the star. The z-axis is directed along the line connecting the center of the star with the observer, and the p-axis is perpendicular to the line of sight. A dimensionless frequency parameter, x, equal to v_z/v_∞, will be used throughout the discussion. The observed line extends from $x = -1$ to $x = +1$.

The loci of points in the envelope with a constant value of v_z is called a constant line of sight velocity surface. Each constant velocity surface corresponds to a particular value of x, the frequency displacement from line center. The velocity surfaces for the law given in equation (2) are shown in Figure 1. Emission from these surfaces distributed over the entire envelope contributes to the observed spectral line.

A simple mathematical formula can be derived for the constant velocity surfaces. For a given value of p and x, we want to determine the value of the radius that satisfies the conditions of the velocity surface. The relation between r, p, and z is just $r^2 = p^2 + z^2$. Therefore, we have

$$r^2(1 - \mu^2) - p^2 = 0 \quad , \tag{3}$$

Figure 1: Constant line of sight velocity surfaces for the accelerating velocity law $v = v_\infty(1 - R_*/r)^{1/2}$. The minimum radius of the surface for $x = .9$ is shown.

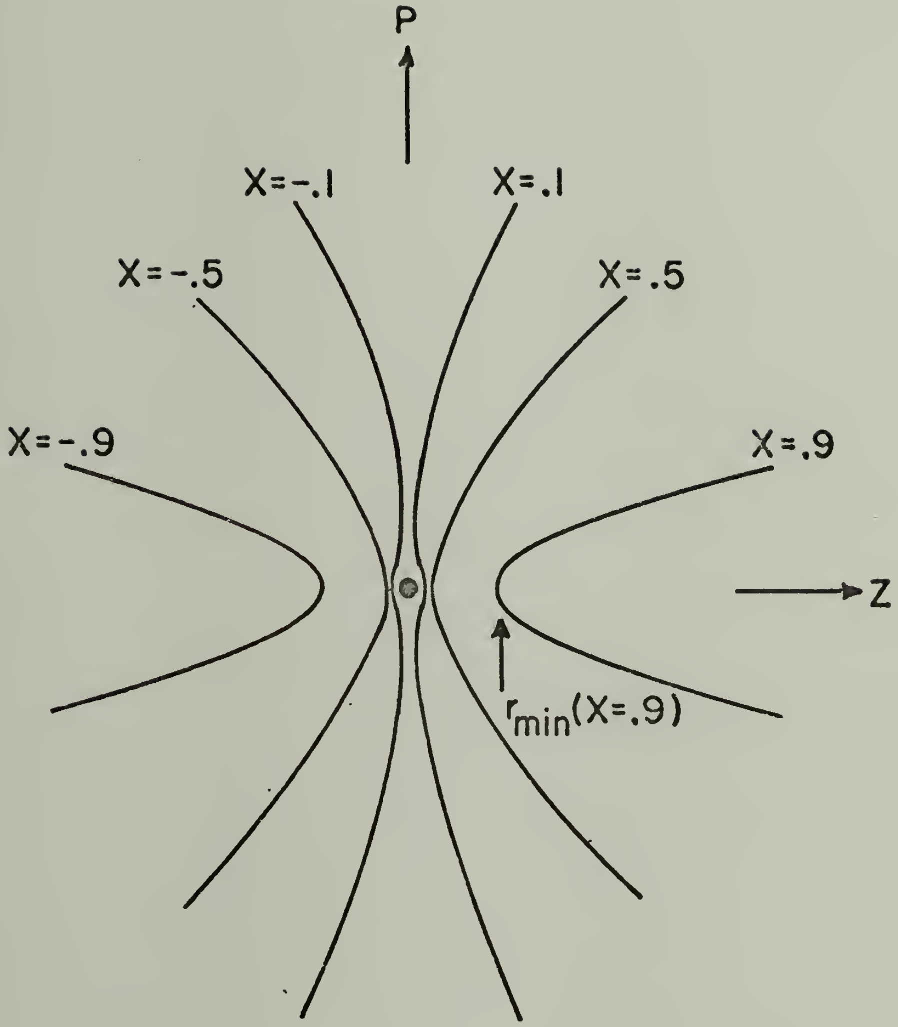
P
X=-.1
X=.1
X=-.5
X=.5
X=-.9
X=.9
Z
$r_{min}(X=.9)$

where $\mu = z/r$. Now, using the definition of x, we have $x = v_z/v_\infty = \mu v/v_\infty$. Equation (3) now becomes

$$r^2(1 - x^2(v_\infty/v)^2) - p^2 = 0 \quad , \tag{4}$$

where v is some function of radius. For the particular velocity law given by equation (2), we have the relation

$$r^2(1 - rx^2/(r - R_*)) - p^2 = 0 \quad . \tag{5}$$

For an accelerating velocity law there will be a minimum radius for a particular velocity surface. In other words, regions close to the star cannot contribute to the flux at large frequency displacements because near the star the gas is moving too slow. For a given value of x, the minimum radius is found by setting $\mu = 1$ in the equation for the definition of x. Since $x = \mu v/v_\infty$, we have $v(r_{min}) = xv_\infty$. For the velocity law given by equation (2), the minimum radius is

$$r_{min} = R_*/(1 - x^2) \quad . \tag{6}$$

Line Profiles

In order to compute line profiles, the intensity and optical depth of a line must be known. For the reader's convenience the functional form of the intensity and optical depth will be given below. Derivations of these relations can be found in the paper by Castor (1970).

In the p-z coordinate system, the intensity and optical depth in a line will be functions of x, p, and z. The intensity seen by the observer, $I(x,p,z=\infty)$, is given by

$$\begin{aligned} I(x,p>R_*,z=\infty) &= S(r_0)(1-\exp(-\tau(x,p,z=\infty))) \\ I(x>0,p<R_*,z=\infty) &= S(r_0)(1-\exp(-\tau(x,p,z=\infty))) \\ &\quad + I_* \exp(-\tau(x,p,z=\infty)) \\ I(x<0,p<R_*,z=\infty) &= I_* \quad , \end{aligned} \tag{7}$$

where $r_0 = (z_0{}^2 + p_0{}^2)^{1/2}$, and the zero subscript refers to a value of a variable on the constant line of sight velocity surface. $S(r_0)$ is the source function in the line at r_0, and I_* is the continuous intensity emitted at R_*. The optical depth in the line is given by

$$\tau(x,p,z=\infty) = \tau_0(r_0)/(1+\sigma z_0{}^2/r_0{}^2) \quad , \tag{8}$$

where

$$\tau_0(r) = \frac{\pi e^2}{mc}\,(gf)_{\ell u}\left(\frac{N_\ell}{g_\ell} - \frac{N_u}{g_u}\right)\frac{rc}{\nu_{\ell u}v(r)} \quad , \tag{9}$$

and

$$\sigma = \frac{d\ln v}{d\ln r} - 1 \quad . \tag{10}$$

The total flux in the line per unit frequency interval is then

$$F_x = 4\pi \int_0^\infty 2\pi p\ I(x,p,\infty)\,dp \quad , \tag{11}$$

and the continuous flux of the star is given by

$$F_c = 4\pi \int_0^{R_*} 2\pi p\, I_*\, dp = 4\pi^2 R_*{}^2 I_* \quad , \tag{12}$$

assuming no limb darkening of the stellar radiation.

Features of Other Velocity Laws

Two other velocity distributions of importance are the laws $v \propto r$

and $v \propto r^{-1/2}$. In this section, the necessary equations will be given for computing the constant velocity surfaces which are shown in Figure 2. The effect of these two velocity laws on the emergent profile will also be discussed.

First, consider the accelerating law

$$v = v_0(r/R_*) \quad , \tag{13}$$

where v_0 is the velocity of the gas at the stellar surface. For purposes of computation, v_0 is usually taken to be the thermal velocity at the stellar surface. The definition of x has to be modified because there is no terminal velocity in the flow. So, we assume that the gas accelerates up to a maximum velocity, v_{max}. Then, the frequency parameter is

$$x = \mu v/v_{max} = \mu\alpha r/R_* \quad , \tag{14}$$

where $\alpha = v_0/v_{max}$.

Solving equation (14) for μ, and substituting into equation (3) results in the relation:

$$z = xR_* \, v_{max}/v_0 \quad . \tag{15}$$

So, for a given value of x, z is a constant independent of p. The resulting velocity surfaces are therefore straight vertical lines, as shown in Figure 2a. Consequently, the value of r_{min} for a given value of x is just the same as the value of z given in equation (15).

Now, we turn to the decelerating velocity law

$$v = v_{max}(R_*/r)^{1/2} \quad , \tag{16}$$

where v_{max} is the velocity of the gas at $r = R_*$. Unlike the previous

Figure 2a: Constant line of sight velocity surfaces for the accelerating velocity law $v = v_o r/R_*$.

Figure 2b: Constant line of sight velocity surfaces for the decelerating velocity law $v = v_{max}(R_*/r)^{1/2}$.

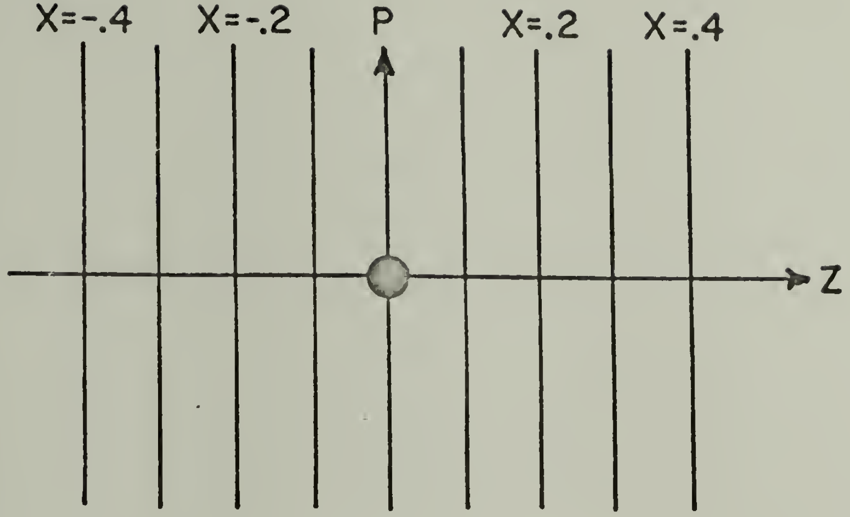
X=-.4
X=-.2
P
X=.2
X=.4
Z

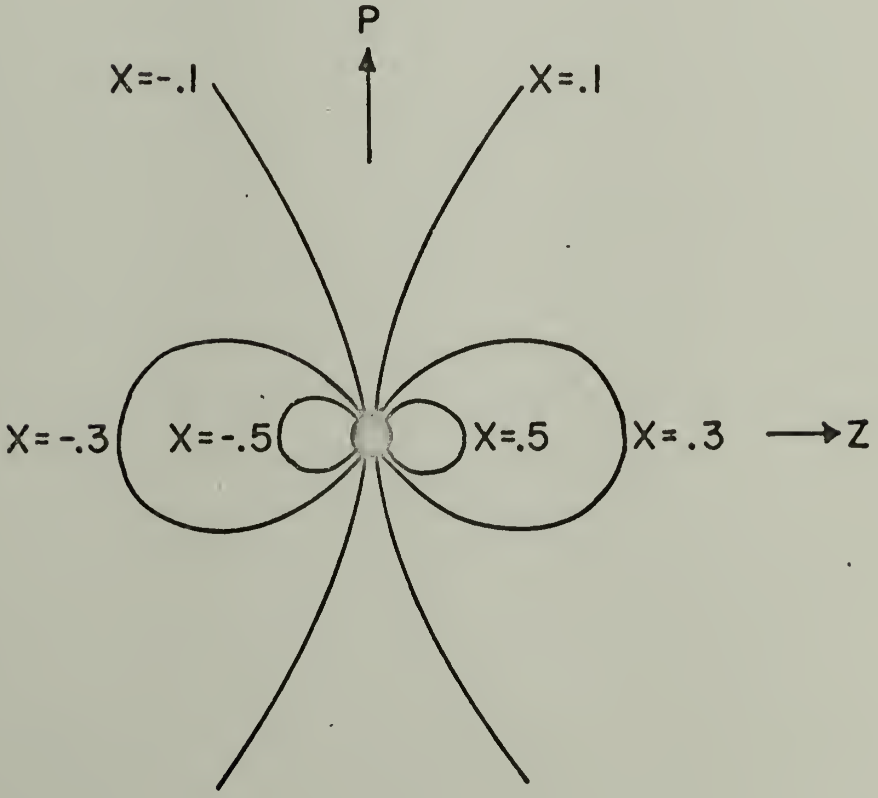
P
X=-.1
X=.1
X=-.3
X=-.5
X=.5
X=.3
Z

velocity laws, this decelerating flow has velocity surfaces that do not extend to infinity, but are closed surfaces as shown in Figure 2b. This means that for a given value of p and x, there are two values of the radius that are on the constant velocity surface. These values are the positive, real, nonzero roots of the equation

$$r^3 + Ar^2 + B = 0 \quad , \tag{17}$$

where $A = -R_*/x^2$ and $B = -Ap^2$.

Now we turn to the differences in the line profiles produced by the three different velocity laws that have been discussed above. The salient features of any accelerating velocity law are: (1) for a given value of x, there is a minimum distance of the velocity surface from the star, and (2) photons emitted from any spot on the disk of the central star must pass through all of the velocity surfaces before reaching the observer. Just the opposite is true for the decelerating velocity law. As shown in Figure 2b, for values of $x \gtrsim .6$, the velocity surfaces do not occult the entire disk of the star. Also, every velocity surface passes through the surface of the star (i.e. there is no minimum radius).

These features have a drastic effect on the resultant line profile. For the decelerating envelope, there will be a cutoff in the flux on the red side of the line at $x \approx -.62$. For values of $x \lesssim -.62$, the stellar disk entirely occults the velocity surfaces. For a given mass loss rate, the intensity of the central emission peak produced by a decelerating flow will be larger than that for an accelerating flow, because the equation of continuity requires that the density, and consequently the source function, decrease less rapidly with radius. For the decelerating flow, the line profiles will also tend to have absorption features at large violet displacements, because the velocity surfaces for large values of x are near the star where the optical depth is large. Also, at these large violet displacements, the surface area of the velocity contours are small, thereby making the total emission only slightly larger than the continuum.

On the other hand, rapidly accelerating velocity laws such as equation (2) cannot give rise to a profile with a large central intensity and a deep, violet displaced absorption feature. If the mass loss rate is increased enough to give a large central intensity, then the resulting emission will completely fill in the absorption feature and a "parabolic" emission line will result. This will be considered in slightly more detail in a later chapter.

CHAPTER III

WOLF-RAYET STARS

A One Point Model For MR 119

The general properties of Wolf-Rayet stars have been summarized in Chapter I. In this chapter, a detailed model for MR 119 is developed in order to calculate the intensities of the neutral helium lines, and thereby infer the temperature in the envelope and the mass loss rate from the star. MR 119 seems to be a fairly good representative of the WN8 stars and is used throughout this work because of the availability of observed line intensities.

The spectrum of HeI (see Figure 3) is different from hydrogenic atoms because transitions between angular momentum substates are observed as distinct lines. Therefore, all of the angular momemtum substates will be included in the model atom. The transitions observed in MR.119 are between levels with $n \leq 8$, so at least this many levels need be included.

Griem (1963) has given a condition for determining which levels of a hydrogenic atom are nearly in LTE by comparing radiative and collisional rates into and out of a certain level. The population of a level n will be within ten percent of its LTE value when $n \geq n_0$, where

$$n_0 = \left[\frac{7.4 \times 10^{18}\ Z^6}{N_e} \left(\frac{kT_e}{E_H}\right)^{1/2}\right]^{2/17} \quad . \tag{18}$$

E_H is the ionization potential of hydrogen, T_e is the local electron temperature, N_e is the electron number density and $Z = 1$ for HeI. For the typical values found in WN envelopes (i.e. $N_e = 10^{11}\ \mathrm{cm}^{-3}$ and

Figure 3: Term diagram for HeI showing the wavelengths of some of the transitions commonly observed in Wolf-Rayet spectra.

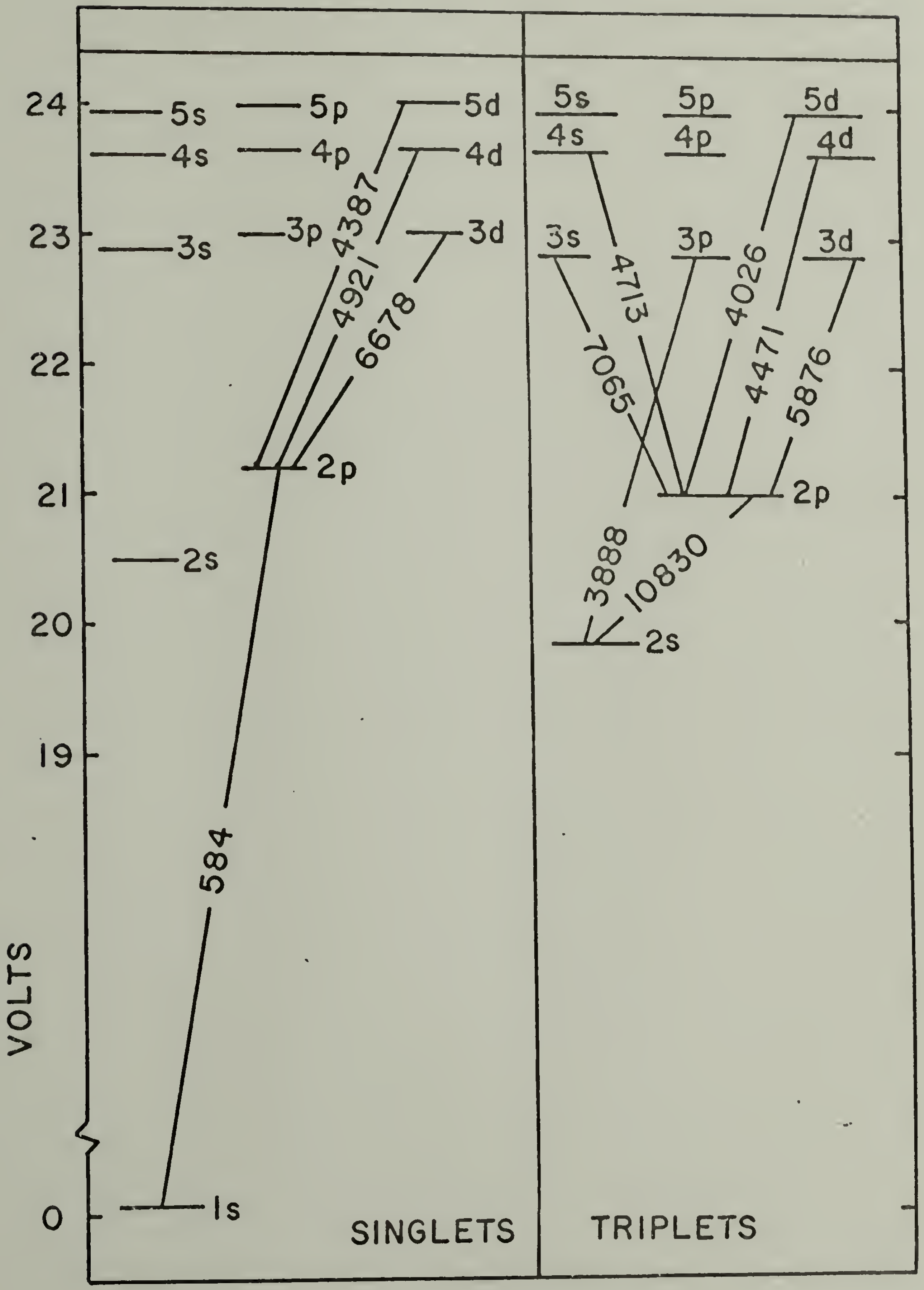
VOLTS
24
23
22
21
20
19
0
5s
4s
3s
2s
1s
5p
4p
3p
2p
5d
4d
3d
4387
4921
6678
584
SINGLETS
5s
4s
3s
5p
4p
3p
5d
4d
3d
2p
2s
4713
7065
4026
4471
5876
3888
10830
TRIPLETS

$T_e = 10^4$ K), we find $n_0 \approx 10$. Although equation (18) is strictly valid only for hydrogenic atoms, its use for neutral helium should not be too severe. Consequently, a neutral helium atom consisting of the first eight principal quantum states including all angular momentum sublevels will be adopted, because of the availability of atomic rates up to n=8.

In order to calculate the populations of these levels, the statistical equilibrium equations must be solved. In a steady state,

$$\frac{dN_{n\ell}}{dt} = R_{n\ell} + C_{n\ell} = 0 \quad , \tag{19}$$

where $R_{n\ell}$ and $C_{n\ell}$ are the net radiative and collisional rates, respectively, by which level $n\ell$ is populated. The net collisional rate is given by

$$\begin{aligned} C_{n\ell} = & \sum_{n \neq n'} \sum_{\ell' = \ell \pm 1} (N_e N_{n'\ell'} C_{n'\ell',n\ell} - N_e N_{n\ell} C_{n\ell,n'\ell'}) \\ & + \sum_{\ell' = \ell \pm 1} (N_c N_{n\ell'} C_{n\ell',n\ell} - N_c N_{n\ell} C_{n\ell,n\ell'}) \\ & + N_e (N_i N_e \gamma_{n\ell} - N_{n\ell} C_{n\ell,k}) \quad , \end{aligned} \tag{20}$$

where N_i is the ion number density, and $C_{n'\ell',n\ell}$, $C_{n\ell,k}$ and $\gamma_{n\ell}$ are the collisional bound-bound, bound-free and three body recombination coefficients. $C_{n\ell',n\ell}$ is the coefficient of collisional redistribution of angular momentum, and N_c is the number density of the species causing this redistribution. N_c will be the density of electrons, protons, or helium ions. The methods used to calculate these collisional rates are given in the Appendix.

The net radiative rate can be written in the form

$$R_{n\ell} = \sum_{n'>n} \sum_{\ell'=\ell\pm1} (N_{n'\ell'}A_{n'\ell',n\ell} + (N_{n'\ell'}B_{n'\ell',n\ell} - N_{n\ell}B_{n\ell,n'\ell'})\bar{J}_{n'\ell',n\ell})$$

$$- \sum_{n'<n} \sum_{\ell'=\ell\pm1} (N_{n\ell}A_{n\ell,n'\ell'} + (N_{n\ell}B_{n\ell,n'\ell'} - N_{n'\ell'}B_{n'\ell',n\ell})\bar{J}_{n\ell,n'\ell'})$$

$$+ N_e N_i \alpha_{n\ell} - 4\pi N_{n\ell} \int_{\nu_{n\ell}}^{\infty} \frac{a_{n\ell}(\nu)}{h\nu} J_\nu(1 - \exp(-h\nu/kT_e)/b_{n\ell})d\nu \quad , \qquad (21)$$

where $\alpha_{n\ell}$ is the radiative recombination rate to level $n\ell$, $a_{n\ell}(\nu)$ is the photoionization cross section from level $n\ell$, $b_{n\ell}$ is the departure coefficient, and J_ν is the mean intensity of the continuous radiation field. The $A_{n'\ell',n\ell}$ and $B_{n'\ell',n\ell}$ are the usual Einstein coefficients, and $\bar{J}_{n'\ell',n\ell}$ is the specific intensity of the radiation field in the transition $n'\ell' \rightarrow n\ell$ integrated over the line profile and average over angle.

Equation (21) can be rewritten in terms of the escape probability of a photon. Castor (1970) showed that the mean intensity, $\bar{J}_{n'\ell',n\ell}$, in an expanding envelope is given by

$$\bar{J}_{n'\ell',n\ell} = (1-\beta)S_{n'\ell',n\ell} + \beta_c I_* \quad , \qquad (22)$$

where β and β_c are escape probabilities defined as:

$$\beta = (1 - \exp(-\tau_{n'\ell',n\ell}(r)))/\tau_{n'\ell',n\ell}(r) \quad , \qquad (23)$$

$$\beta_c = W\beta \quad . \qquad (24)$$

The term β_c is the probability that a photon will escape from the region in which it was emitted and strike the central star or core. In the above equations, W is the dilution factor, I_* is the intensity of the core, and $S_{n'\ell',n\ell}$ is the source function in the line and is given by

$$S_{n'\ell',n\ell} = N_{n'\ell'}A_{n'\ell',n\ell}/(N_{n\ell}B_{n\ell,n'\ell'} - N_{n'\ell'}B_{n'\ell',n\ell}) \quad . \qquad (25)$$

By substituting equation (25) into equation (22), the mean intensity, $\bar{J}_{n'\ell',n\ell}$, can be written solely in terms of atomic rates and escape probabilities. The net radiative rate given by equation (21) can now be expressed in the following form:

$$\begin{aligned} R_{n\ell} = & \sum_{n'>n} \sum_{\ell'=\ell\pm1} (N_{n'\ell'}A_{n'\ell',n\ell}\beta + (N_{n'\ell'}B_{n'\ell',n\ell} - N_{n\ell}B_{n\ell,n'\ell'})\beta_c I_*) \\ & - \sum_{n'<n} \sum_{\ell'=\ell\pm1} (N_{n\ell}A_{n\ell,n'\ell'}\beta + (N_{n\ell}B_{n\ell,n'\ell'} - N_{n'\ell'}B_{n'\ell',n\ell})\beta_c I_*) \\ & + N_e N_i \alpha_{n\ell} - 4\pi N_{n\ell} \int_{\nu_{n\ell}}^{\infty} \frac{a_{n\ell}(\nu)}{h\nu} J_\nu (1 - \exp(-h\nu/kT_e)/b_{n\ell}) d\nu \quad . \qquad (26) \end{aligned}$$

Methods used to calculate the atomic rates are listed in the appendix. Also, the simplified method used by Castor and Van Blerkom (1970) to deal with the continuum radiation will be adopted here.

Now, with the net radiative and collisional rates being given by equations (26) and (20), respectively, the rate equation (19) can be written in matrix form

$$\underset{\approx}{A}\,\underset{\sim}{X} = \underset{\sim}{B} \quad , \qquad (27)$$

where $\underset{\approx}{A}$ is a matrix containing escape probabilities and $\underset{\sim}{X}$ is a vector whose elements are the populations of the levels. Equation (27) is solved by an iterative method. The populations of the levels are initially guessed to be their LTE values for the local electron temperature. Then, using equations (9) and (23), the optical depths and escape probabilities in the lines are calculated. This completely determines matrices $\underset{\approx}{A}$ and $\underset{\sim}{B}$ in equation (27). The new populations, contained in vector $\underset{\sim}{X}$, are then found by calculating the product $\underset{\sim}{B}\,\underset{\approx}{A}^{-1}$. This process is repeated until the populations of all levels converge. In practice, the fractional change in the populations of all levels is less than 1% after only three or four iterations.

So, after equation (27) has been solved, the populations of the levels of neutral helium are known at one point in the envelope. The populations can now be used to calculate the total intensity of an emission line. The intensity of the transition $n'\ell' \rightarrow n\ell$ is given by

$$I_{n'\ell',n\ell} \propto \int j(r)\beta(r)dV \quad , \tag{28}$$

where $j(r)$ is the emission coefficient and V is the volume. Using the relations $j(r) = k(r)S(r)$ and from equation (9)

$$k(r) = \tau_{n\ell,n'\ell'}\, v(r)\nu/rc \quad , \tag{29}$$

equation (28) becomes

$$I_{n'\ell',n\ell} \propto \int S(r)\, \frac{\nu_o v(r)}{cr}\, (1 - \exp(-\,\tau_{n\ell,n'\ell'}(r)))dV \quad . \tag{30}$$

This integral cannot be evaluated correctly without knowing the run of physical parameters over the whole volume of the envelope. Since the calculations have been performed at only one point in the envelope, the integral can be approximated by assuming that $S(r)(1 - e^{-\tau})$ is constant for $r < R$ and zero for $r > R$. Then,

$$I_{n'\ell',n\ell} = K\, \frac{\nu_o^{\,4}(1 - \exp(-\,\tau_{n'\ell',n\ell}))}{(\frac{N_\ell\, g_u}{N_u\, g_\ell} - 1)} \quad , \tag{31}$$

where K is a constant. In order to eliminate this constant, the intensities will be given in terms of a reference intensity. The reference lines are $2^3P - 4^3D$ (λ4471) and $2^1P - 4^1D$ (λ4922) for the triplets and singlets, respectively. These lines were chosen because they are present in the spectrum of MR 119, and they are relatively free of blends.

We now apply this model to MR 119, a representative WN8 star. MR 119 has a core temperature of ∿ 23,000 K and H/He ∿ 1 (Smith 1972). The bolometric magnitude of a WN8 star is -8.5 (Smith 1972), which corresponds to $\log(L/L_\odot) = 5.3$ where $L = 4\pi R_*^2 \sigma T_*^4$. Using a core temperature of 23,000 K gives a radius of $R_* \gtrsim 30\ R_\odot$. The representative point in the envelope where the rate equations are solved is chosen to be $R = 3R_* = 90\ R_\odot$ and the velocity of the gas at this point is assumed to 1000 km s^{-1}. These choices have very little effect on the computed line intensities.

The two remaining parameters that must be chosen are the temperature and density of the gas at the representative point. If the stellar mass loss rate is $10^{-5}\ M_\odot\ \mathrm{yr}^{-1}$, then using $R = 90\ R_\odot$, $v(R) = 1000$ km s^{-1}, and the equation of continuity, we find that the number density of helium is roughly 10^{10} cm^{-3} at this point. With this rough estimate of the particle density in mind, eight models were computed corresponding to two values of the electron temperature: $T_e = 1$ and 2×10^4 K; and four values of the helium density: N(He) = 2, 3, 5 and 7 x 10^{10} cm^{-3}.

The calculated and observed relative intensities are shown in Table I for both singlet and triplet transitions. All the observed relative intensities are taken from the Atlas of Wolf-Rayet Line Profiles (Kuhi and Smith 1972), except for the intensity of the $2^3P - 2^3S$ transition which is taken from Kuhi (1968).

In Figure 4, the logarithm of the departure coefficient is plotted versus the principal quantum number, n, for the $\ell = 0$ state for two tem-

TABLE I′

Singlet and Triplet Line Intensities Relative to $I(4^1D - 2^1P)$ and $I(4^3D - 2^3P)$, Respectively

$N(He)(cm^{-3})$...	2×10^{10}		3×10^{10}		5×10^{10}		7×10^{10}		
Temperature...	10^4	2×10^4	10^4	2×10^4	10^4	2×10^4	10^4	2×10^4	Observed
$I(5^1D - 2^1P)$	.41	.41	.53	.46	.65	.60	.68	.66	.65
$I(6^1D - 2^1P)$	.21	.20	.28	.24	.45	.36	.56	.48	.63
$I(5^3D - 2^3P)$	.59	.51	.66	.61	.66	.65	.69	.67	.90*
$I(6^3D - 2^3P)$	.34	.25	.47	.35	.55	.51	.61	.59	.30
$I(7^3D - 2^3P)$	.21	.16	.32	.23	.49	.41	.58	.53	.42*
$I(8^3D - 2^3P)$	.14	.10	.23	.16	.42	.32	.55	.49	.33
$I(4^3S - 2^3P)$	.23	.19	.40	.28	.72	.55	.86	.75	.43
$I(3^3P - 2^3S)$	1.64	1.74	1.87	1.74	2.38	2.30	2.61	2.80	3.02*
$I(2^3P - 2^3S)$	1.35	1.40	1.33	1.44	1.30	1.57	1.25	1.61	2.88

Note: An asterisk denotes a blended line

Figure 4: The logarithm of the departure coefficient, $b_{n\ell}$, is plotted against the principal quantum number for triplet states with $\ell = 0$. Curve (a) is for T = 20,000 K and N(He) = 5×10^{10} cm^{-3}, and curve (b) is for T = 10,000 K and N(He) = 3×10^{10} cm^{-3}.

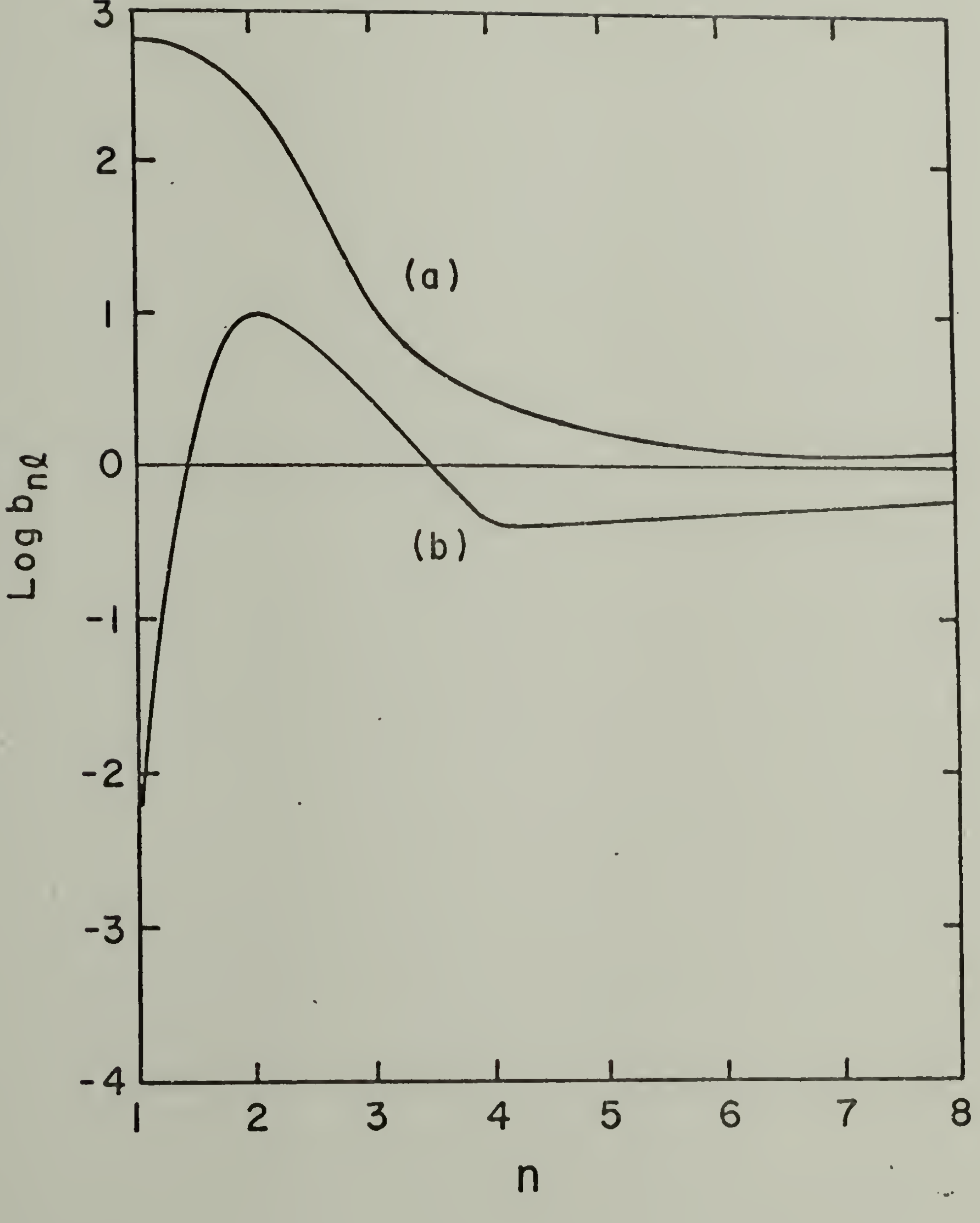

3
2
1
0
-1
-2
-3
-4
Log $b_{n\ell}$
(a)
(b)
1
2
3
4
5
6
7
8
n

peratures and densities. The departure coefficient falls to approximately unity as $n \rightarrow 8$, verifying the assumption made earlier that levels above $n = 8$ would be within ten percent of LTE.

It is difficult to interpret the results from Table I. Therefore, for purposes of clarification, some of the relative intensities from Table I are plotted in Figure 5 for the two different temperatures for the $n^3D - 2^3P$ series of transitions. The observed values are also shown. On the basis of this graph there does not seem to be a unique solution for the temperature and density in the envelope. For an envelope temperature of 20,000 K a density of 5-7 x 10^{10} cm^{-3} fits best, whereas for 10,000 K a density of 2-3 x 10^{10} cm^{-3} is indicated. The scatter in the observed intensities, partially caused by line blending, makes it very difficult to rule out one of these two sets of temperatures and densities. However, we can eliminate one of these sets by studying the other observed lines.

Consider first the singlet lines. Even though there are only two singlet lines present in the spectrum (and the intensity of $5^1D - 2^1P$ transition is uncertain), the calculated intensities for the high density (7×10^{10} cm^{-3}) case are in good agreement with the observed values. There is not much difference, however, between the calculated values for 10,000 K and those for 20,000 K. Therefore, the two singlet lines are consistent with the high density and high temperature case, but not with the low density - low temperature case.

Two of the strongest lines observed in MR 119 are the $\lambda3889$ ($3^3P - 2^3S$) and $\lambda10830$ ($2^3P - 2^3S$) lines. The calculated result for $\lambda3889$ is in very good agreement with the observed intensity for the case with a total

Figure 5: The intensity of the transitions $n^3D - 2^3P$ relative to the intensity of the transition $4^3D - 2^3P$ is plotted as a function of n ($4 \leq n \leq 8$). Curves (a), (b), (c), and (d) are for total helium densities of 7, 5, 3, and 2×10^{10} cm^{-3}, respectively. Curves (a) and (b) are for $T = 20{,}000$ K while curves (c) and (d) are for $T = 10{,}000$ K. Observed values appear as encircled dots.

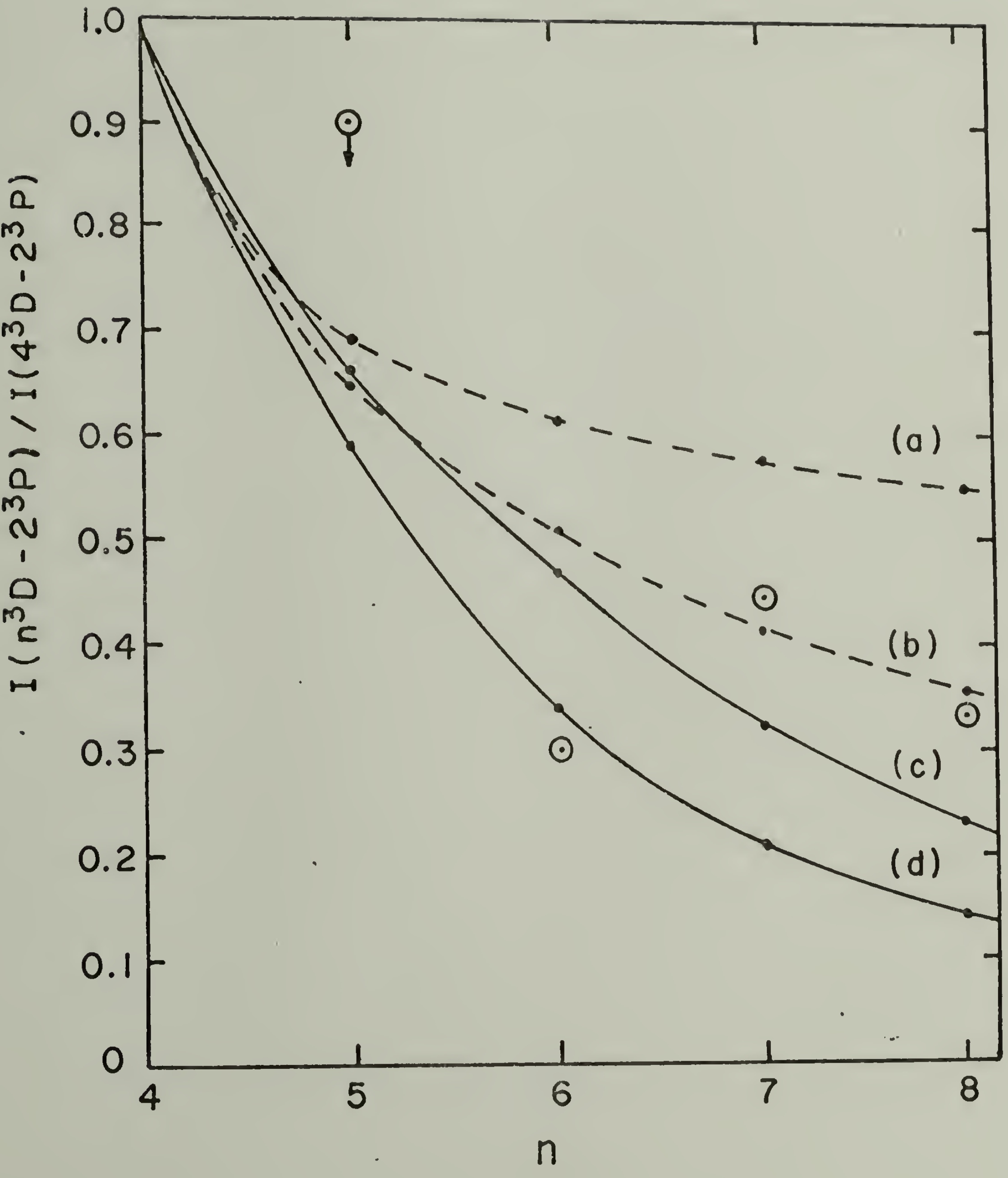
I(n³D-2³P) / I(4³D-2³P)
1.0
0.9
0.8
0.7
0.6
0.5
0.4
0.3
0.2
0.1
0
4
5
6
7
8
n
(a)
(b)
(c)
(d)

helium density of $\sim 7 \times 10^{10}$ cm^{-3}. Again, there is not much difference between the calculated intensities for the two different temperatures. Although the λ3889 line is blended with a hydrogen line and an ionized helium line at roughly the same wavelength, these lines contribute only slightly to the intensity of the HeI line. Not any of the calculated intensities for λ10830 are close to the observed value, indicating that the idea of a representative emitting point in the envelope may be breaking down.

On the whole, a temperature of 20,000 K and a total helium density of 5-7 x 10^{10} cm^{-3} at $R = 3R_*$ seems to be consistent with the observations. The most serious approximation made in this calculation was the assumption of homogeneity. Obviously, the temperature and density are not constant everywhere in the envelope. By taking values of temperature, density, and velocity at one point as being representative of the whole envelope, calculated intensities of some lines may be in error by a factor of two or more. However, the use of homogeneity gives results that agree rather well with observation and simplifies the calculations immensely. Besides, a more detailed approach for MR 119 is not warranted because of the probable errors in the observed line intensities.

Castor and Van Blerkom (1970) found that the temperature in the envelope was greater than the core temperature for HD 192163, which means that some kind of mechanical energy input is required to keep the envelope hotter than the core. For MR 119, we find that $T_e \lesssim T_*$ indicating that a source of mechanical energy is not required and that the envelope may be in radiative equilibrium.

A total helium density of 5-7 x 10^{10} cm^{-3} at $R = 90\ R_\odot$ gives a mass loss rate of $\sim 10^{-4}$ $M_\odot$ yr^{-1}. The usual range of mass loss rates quoted for Wolf-Rayet stars is 10^{-6} - 10^{-4} $M_\odot$ yr^{-1}, putting MR 119 on the upper end of this spectrum.

CHAPTER IV

P CYGNI

Previous Observations and Interpretations

As pointed out in the introduction, two of the most recent studies of P Cygni have reached different conclusions regarding the velocity distribution in the surrounding envelope. A brief summary of the arguments for and against an accelerating flow are given below.

It has been known for a long time that there is a definite correlation between the displacement of the absorption edge of a line and the excitation potential of the absorbing ion (Beals 1935, Struve 1935). In general, the radial velocity obtained from the displacement of the absorption is larger for lines arising in ions of lower total excitation energy (ionization potential + excitation potential). Thus, ions with large total excitation energy exist in a more slowly moving region of the atmosphere than those with small total excitation energy. If there is no temperature inversion in the atmosphere, it follows that the material velocity increases with radius, i.e. the flow is "accelerated".

As discussed in the introduction, de Groot (1969) reported that the hydrogen Balmer lines have violet displaced absorption features that show three distinct components. The component furthest to the blue shows a periodic variation in radial velocity of 114 days. If this absorption component is formed in a particular portion of the envelope (for instance, in a shell) the absorption region is most likely far from the star. If it was near the star, then it would be hard to explain why this region varied periodically and the outer regions did not. So, the fact that only the most violet displaced absorption component shows this variation is evidence that the outermost regions of the atmosphere expand the fastest.

Recent infrared observations of P Cygni have been made by Wright and Barlow (1975) and Barlow and Cohen (1977). The excess infrared flux from P Cygni is almost certainly due to thermal free - free emission from the circumstellar ionized gas. Now, the linear free - free absorption coefficient is a function of the gas number density, which in turn is a function of the velocity distribution in the envelope via the equation of continuity. Therefore, the flux density - frequency relation for the emitted free - free radiation will vary depending on the velocity law in the circumstellar envelope. For the three velocity laws, (1) $v \propto r^{-1/2}$, (2) $v = \text{constant}$, (3) $v \propto r$, Wright and Barlow (1975) find the following flux density - frequency relations: (1) $S = \text{constant}$, (2) $S \propto \nu^{2/3}$ and (3) $S \propto \nu^{6/5}$, respectively. If the gaunt factor is included, then the spectral indices will be decreased by about .1. The spectral index found for P Cygni by joining the radio and infrared fluxes between 10 GHz and 10 μ is .75. This spectral index indicates that the flow is accelerating slowly.

The three lines of evidence presented above tend to give the accelerating flow hypothesis quite a bit of credibility. However, Kuan and Kuhi (1975) have pointed out two features of the hydrogen Balmer lines that indicate a decelerating flow. First, the early Balmer lines have strong central emission (up to 12 times the continuum intensity for Hα), but absorption components that reach nearly to zero. Second, the red side of the emission components of these lines have a cut-off at $x \approx -.6$. Both of these features are easily produced by a decelerating flow, as discussed in Chapter II. An accelerating flow model with the velocity law $v(r) = v_\infty(1 - R_*/r)^{1/2}$ cannot produce the observed Hα profile, because the strong envelope emission necessary to account for the central intensity will fill in the absorption trough, producing only a weak absorption feature. Faced with the substantial differences between de Groot's interpretation of P Cygni and that of Kuan and Kuhi, both based on an analysis of hydrogen Balmer lines, we decided to look at the rich HeI spectrum to see whether a consistent model could be obtained from this ion.

A Model for the He I Spectrum

The neutral helium line profiles have a very different appearance than the Balmer lines (Adams and Merrill 1957). The central intensities are quite small and the absorption features are usually much closer to line center. The smaller emission intensities suggest that an accelerating flow has a good chance of being able to produce the helium lines.

Since the process by which mass is being ejected from P Cygni is not known, the velocity law in the envelope is not known. Nevertheless, assume that the gas is being accelerated outward from the surface by some unknown force that produces an acceleration of α times the gravitational acceleration. If g is the acceleration of gravity at the stellar radius R_*, the equation of motion is

$$\ddot{r} = (\alpha - 1)\, g\, (R_*/r)^2 \quad . \tag{32}$$

Integrating this equation gives the velocity law

$$v(r) = [v^2(R_*) + v_\infty{}^2(1 - R_*/r)]^{1/2} \quad , \tag{33}$$

which is identical to equation (2) with $v(R_*) = 0$.

The density of helium at any point in the envelope, $N_{He}(r)$, is determined by the equation of continuity. If Y is the mass fraction of helium, then

$$N_{He}(r) = Y\dot{M}/(4\pi r^2 m_{He} v(r)) \quad . \tag{34}$$

The temperature distribution of the gas in the envelope is unknown and will have to be assumed. For the following calculation, it was assumed that the temperature of the gas decreased radially as $r^{-1/2}$. However, it was found that the exact temperature distribution was relatively unimportant as far as the emergent line profiles are concerned.

Using the equations presented above with the method outlined in Chapter II, the profiles of the HeI lines, and their equivalent widths, were constructed with the following additional parameters. The atmosphere is assumed to be composed of only hydrogen and helium in a ratio of 2 to 1 by mass. The terminal velocity of the flow is taken to be 280 km s^{-1}. A static photosphere of radius $R_* = 15.2\ R_\odot$ and temperature $T_* = 30{,}500$ K (Kuan and Kuhi 1975) radiates a continuous spectrum taken to be blackbody at T_*. These parameters, together with the mass loss rate $\dot{M}$, define a model of the line emitting region. A few of the calculated and observed line profiles are shown in Figures 6, 7, and 8.

The peculiarities of the HeI spectrum were first pointed out by Adams and Merrill (1957). While HI lines show absorption components which all have about the same velocity displacement from line center,

Figure 6: Line profile for λ4387. The solid line is the theoretical profile, and the dashed line is the observed profile.

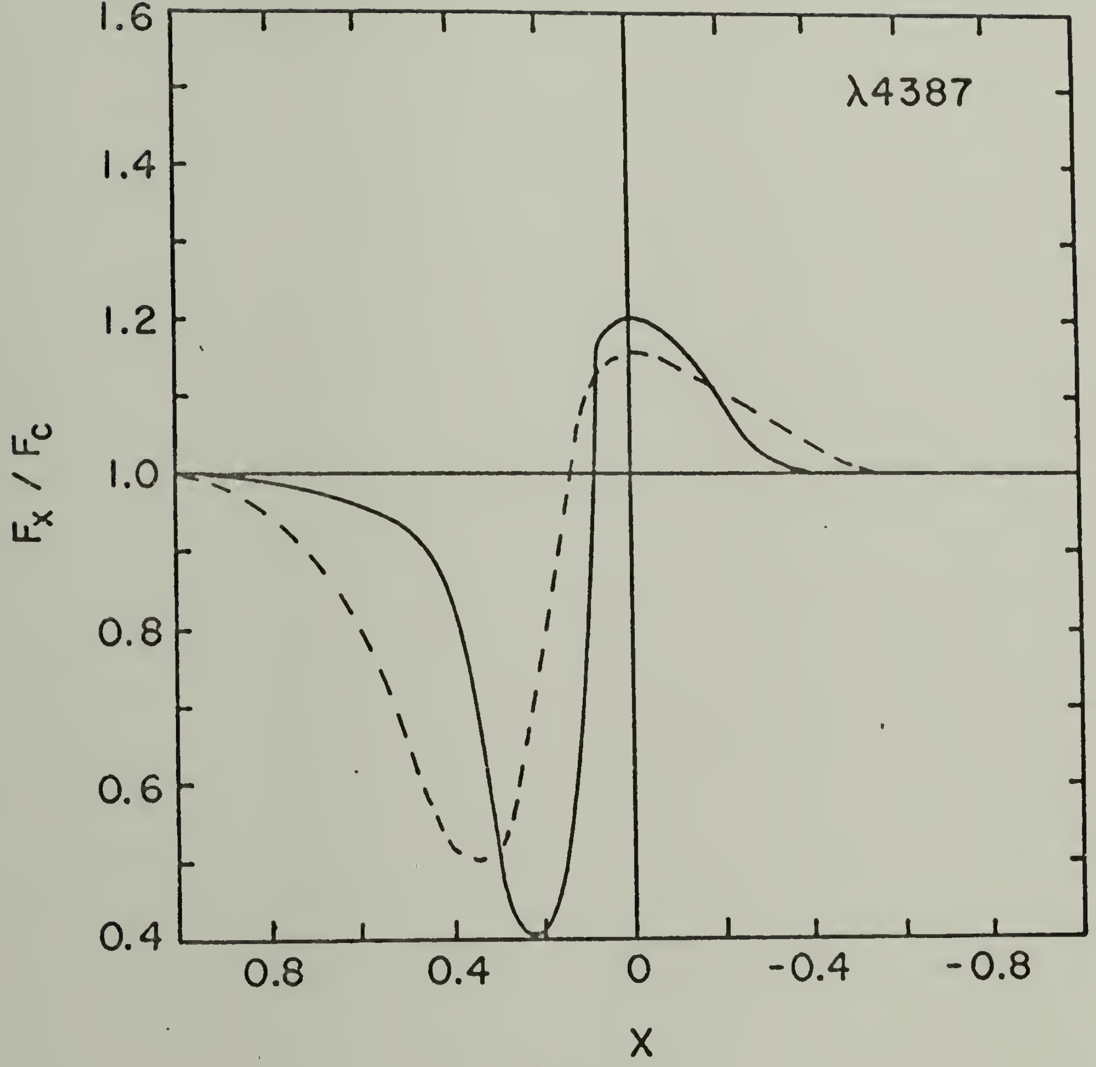
λ4387
1.6
1.4
1.2
1.0
0.8
0.6
0.4
F_x / F_c
0.8
0.4
0
-0.4
-0.8
X

Figure 7: Line profile for λ4026. Curves (a) and (b) are the calculated profiles using $\dot{M} = 3 \times 10^{-6}$ and 2×10^{-6} $M_{\odot}\,yr^{-1}$ respectively. The dashed line is the observed profile.

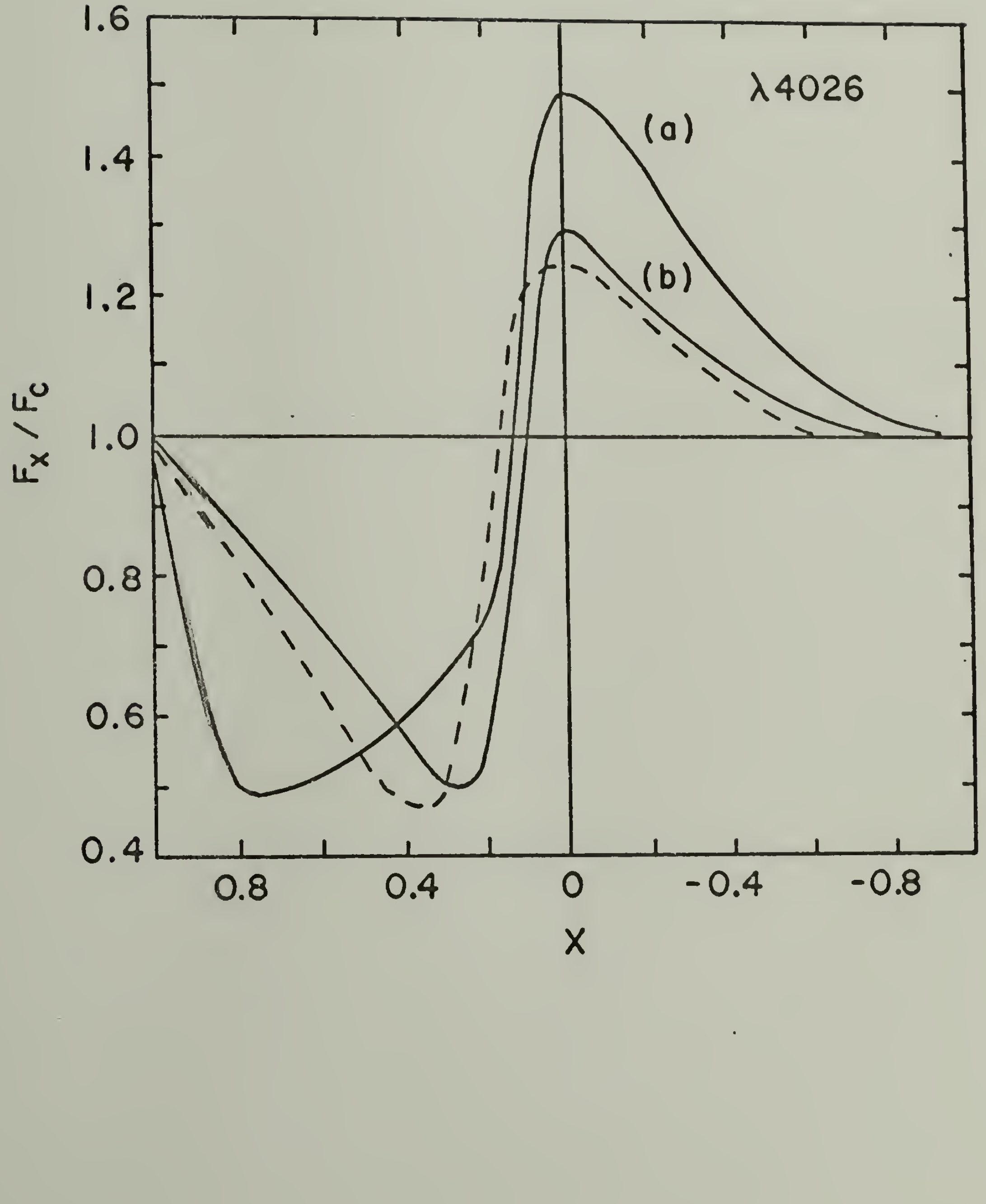
λ4026
(a)
(b)
1.6
1.4
1.2
1.0
0.8
0.6
0.4
F_x / F_c
0.8
0.4
0
-0.4
-0.8
X

Figure 8: Line profile for λ4471. Curves (b) and (c) are the theoretical profiles using $\dot{M} = 2 \times 10^{-6}$ and 1×10^{-6} $M_\odot yr^{-1}$ respectively. Again, the dashed line is the observed profile.

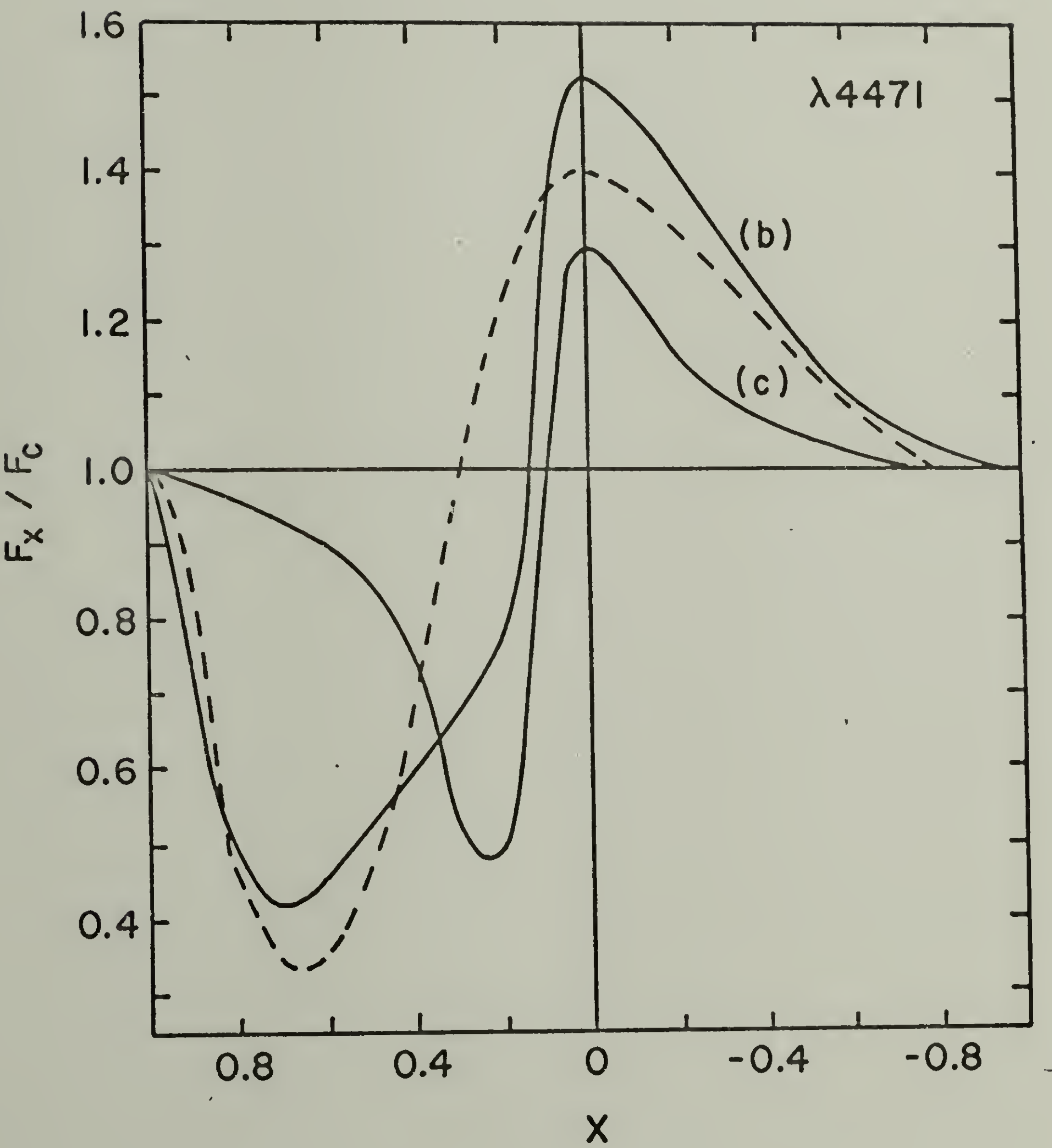
λ4471
(b)
(c)
F_x / F_c
1.6
1.4
1.2
1.0
0.8
0.6
0.4
0.8
0.4
0
-0.4
-0.8
X

HeI absorption components have displacements that vary from line to line. "In general, the strongest helium line in the photographic region, 4471 Å, yields displacements something like those of the hydrogen lines, while weaker lines, even in the same series, yield smaller negative displacements. This peculiar behavior deserves further study." The lines λ4471 and λ4026, shown in Figures 7 and 8, show this effect: the absorption edge of λ4471 has a displacement of ∿ 185 km s^{-1}, while that of λ4026 is only ∿ 110 km s^{-1}. Since this behavior involves the absorption components of the lines, it seems reasonable to assume that this effect is caused by the optical depth in the lines. Therefore, let us consider the effect of a finite optical depth on the emergent line profiles.

The violet absorption component is produced by matter lying in front of the star, where $\mu \approx 1$. The optical depth to a photon in the continuum at a frequency displacement x is, from equation (8), $\tau_o(r_o)/(1+\sigma(r_o))$, where r_o is on the constant velocity surface corresponding to x. Using equations (9) and (10), the optical depth can be written

$$\tau(x,p=0,z=\infty) = \frac{\pi e^2}{mc}\,(gf)_{\ell u}\,\frac{N_\ell}{g_\ell}\,\left(1 - \frac{g_\ell N_u}{g_u N_\ell}\right)\frac{r_c}{v\nu_{\ell u}}\left(\frac{r}{v}\frac{dv}{dr}\right)^{-1} \quad . \qquad (35)$$

Now, using the equation of continuity and ignoring the stimulated emission term in equation (35), we have

$$\tau(x,p=0,z=\infty) = \frac{\pi e^2}{mc}\,(f\lambda)_{\ell u}\,\frac{Y\dot{M}}{2\pi m_{He}}\,\left(f(r)/r^2\,\frac{dv^2}{dr}\right)_{r_o} \quad , \qquad (36)$$

where $f(r) = N_\ell/N_{He}$ is the fraction of neutral helium in the lower level of the transition. Written in this manner, the radial dependence of the optical depth is more clearly seen. For the velocity distribution given by equation (2), equation (36) reduces to $\tau(r) \propto f(r)$. If E_ℓ is the energy of level ℓ above the ground state of neutral helium, and $U_o(T)$ is the partition function, then

$$f(r) = \frac{g_\ell b_\ell \exp(-E_\ell/kT)/U_o(T)}{1 + N_{He^+}/N_{He^o}} , \qquad (37)$$

where doubly ionized helium is assumed to be a negligible constituent. Equation (37) is a very complicated function of radius. The departure coefficient, b_ℓ, the temperature, and the ratio N_{He^+}/N_{He^o} are all functions of radius. However, the behavior of the exponential term probably dominates f(r), so that the optical depth decreases with radius (for instance, for transitions out of the level 2^3P, if $T \propto r^{-1/2}$, $\exp(-E_\ell/kT)$ decreases by a factor of ~ 2000 from $r = R_*$ to $4R_*$). Figure 9 shows the calculated radial dependence of the optical depth for three of the HeI lines.

Absorption of continuum photons becomes significant when $\tau(x,p,z) \simeq 1$. Let us define the radius at which $\tau_{4026} \approx 1$ to be R_{4026} for the λ4026 line. Continuum photons are absorbed in the line from line center, $x = 0$, to $x = v(R_{4026})/v_\infty$. Since the envelope is more opaque to λ4471 radiation, $R_{4471} > R_{4026}$. Again, absorption in the λ4471 line extends from $x = 0$ to $x = v(R_{4471})/v_\infty$. In an accelerating envelope, $v(R_{4471}) > v(R_{4026})$ so absorption extends further to the blue in the λ4471 transition than in λ4026. Of course, the real appearance of the line profile will depend on the emission component (for instance, if the emission is large, there may not be any absorption component at all). Nevertheless, this simple argument suffices to show that two lines may be formed in the same region of the envelope, and yet have different displacements

Figure 9: The logarithm of the optical depths (for $\mu = 1$) in the three lines $\lambda\lambda$4471, 4387, and 4026 is plotted against r, the radial distance from the star.

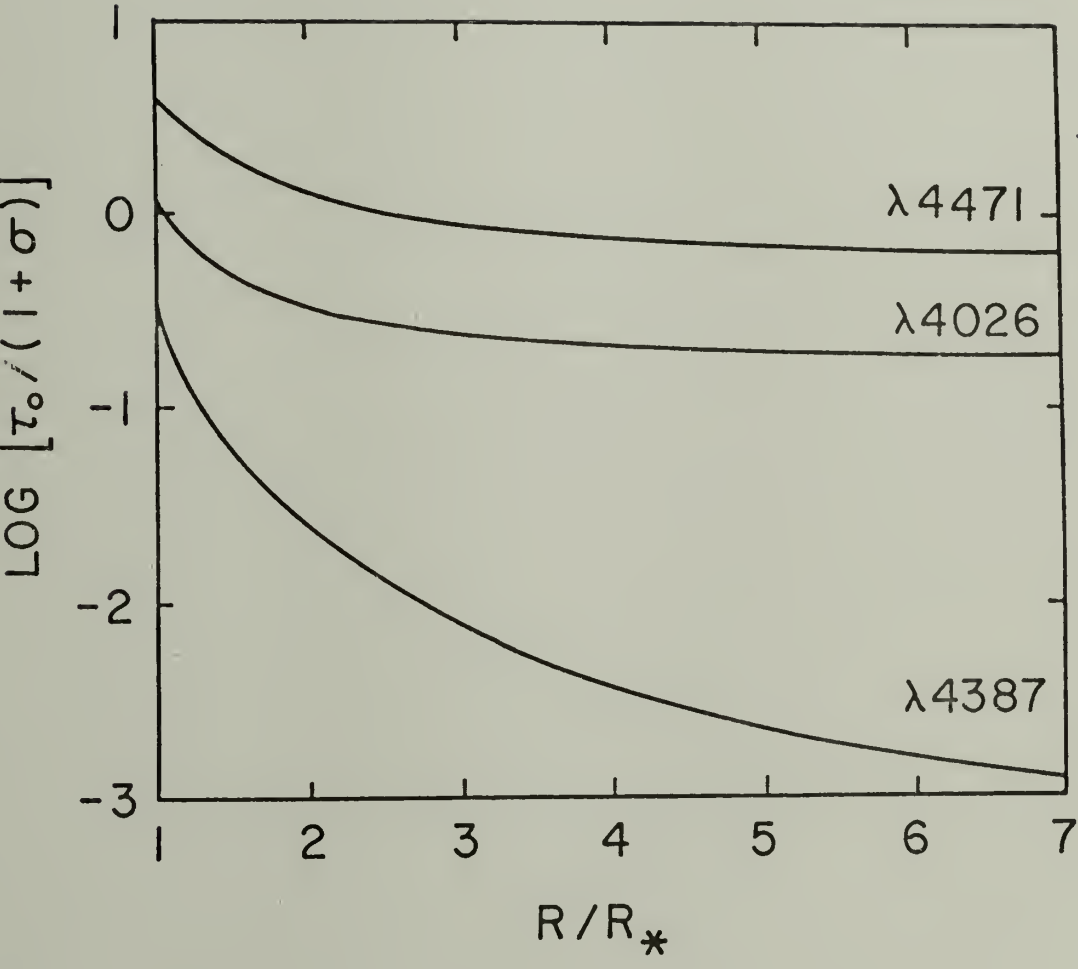
λ4471
λ4026
λ4387
LOG [τ₀/(1+σ)]
1
0
-1
-2
-3
1
2
3
4
5
6
7
R/R*

of their absorption edges from line center if they differ in optical depth.

Equation (36) also states that the optical depth in a line is directly proportional to the mass loss rate from the star. Changing the mass loss rate will therefore change R_{4026} and R_{4471}, thereby changing the positions of the absorption edges, as shown in Figures 7 and 8. For $\dot{M} = 10^{-6}$ $M_\odot$ yr^{-1} both λ4026 and λ4471 are optically thin over most of the envelope, and thus have profiles with absorption components relatively close to line center. When $\dot{M}$ is increased to 3×10^{-6} $M_\odot$ yr^{-1}, the two lines are optically thick for a considerable distance, and give rise to absorption edges with large velocity displacements. Clearly, a mass loss rate between 1 and 3×10^{-6} $M_\odot$ yr^{-1} is required to give a larger violet displacement for λ4471 than for λ4026. Figures 6, 7, and 8 show the results of the line profile computation for $\dot{M} = 2 \times 10^{-6}$ $M_\odot$ yr^{-1}. The agreement between the model calculations and the observed profiles is quite good. The equivalent widths of the absorption components of various lines are listed in Table II. In general, the calculated values are within 20 percent of the observed values. In some cases, e.g. λ4713, the comparison leaves something to be desired, but the overall results are still rather good. Errors in the observed values are estimated by de Groot to be about 15 percent.

Unfortunately, the success of this model is limited, because we cannot infer that the whole envelope is accelerating for the following reason. The weak lines (i.e. λλ4026, 4387) have small velocity shifts of their absorption minima, indicating that these lines are formed near the star. For instance, the absorption minimum for λ4026 is at $x \approx 0.3$,

TABLE II

Equivalent Widths of HeI Absorption Components

Transition	Wavelength (Å)	Calculated E.W. (Å)	Observed* E.W. (Å)
$2^3P - 4^3D$	4471	1.27	1.01
$2^3P - 5^3D$	4026	0.92	0.80
$2^3P - 6^3D$	3819	0.74	0.62
$2^3P - 4^3S$	4713	0.65	0.36
$2^3P - 5^3S$	4120	0.42	0.29
$2^1P - 4^1D$	4921	0.66	0.53
$2^1P - 5^1D$	4387	0.61	0.56
$2^1P - 6^1D$	4143	0.52	0.45
$2^1S - 4^1P$	3964	0.55	0.58
$2^1S - 5^1P$	3613	0.32	0.21

*de Groot (1969)

which corresponds to layers of the envelope at $r \approx 1.1\ R_*$. This shows that the outer portion of the envelope, say, beyond $2R_*$, may not contribute significantly to the formation of the weaker lines. To test this hypothesis, line profiles were constructed exactly as before, but ignoring contributions to the lines from $r \geq 2R_*$, by setting the source functions and optical depths at these points equal to zero. The resultant profiles of the weak lines are not significantly changed, the only difference being a small decrease in the height of the emission peak and shortward and longward cutoffs to the profile. The profile of the stronger line λ4471 is changed to a greater extent, but in general, the deletion of the envelope beyond $2R_*$ does not greatly affect the appearance of the emergent line profiles. Basically, this whole problem is caused by the rapidly accelerating velocity law we have used. The velocity in the envelope approaches the terminal velocity so rapidly that the outer portions of the atmosphere cannot contribute significantly to the line. Therefore, we can conclude that the region in which the HeI lines are formed is expanding with a velocity that increases with radius, but we cannot say with any assurance that the envelope is accelerating at still larger values of radius.

The Double Absorption Features

According to de Groot (1969), the hydrogen Balmer lines have violet displaced absorption features that show more than one component. One of these lines, H10 ($10 \rightarrow 2$), is shown in Figure 10. One of the more puzzling aspects of the double absorption features is their variability. de Groot suggested that these features were caused by absorption in

Figure 10: The observed line profile for Balmer 10, showing the characteristic double absorption components.

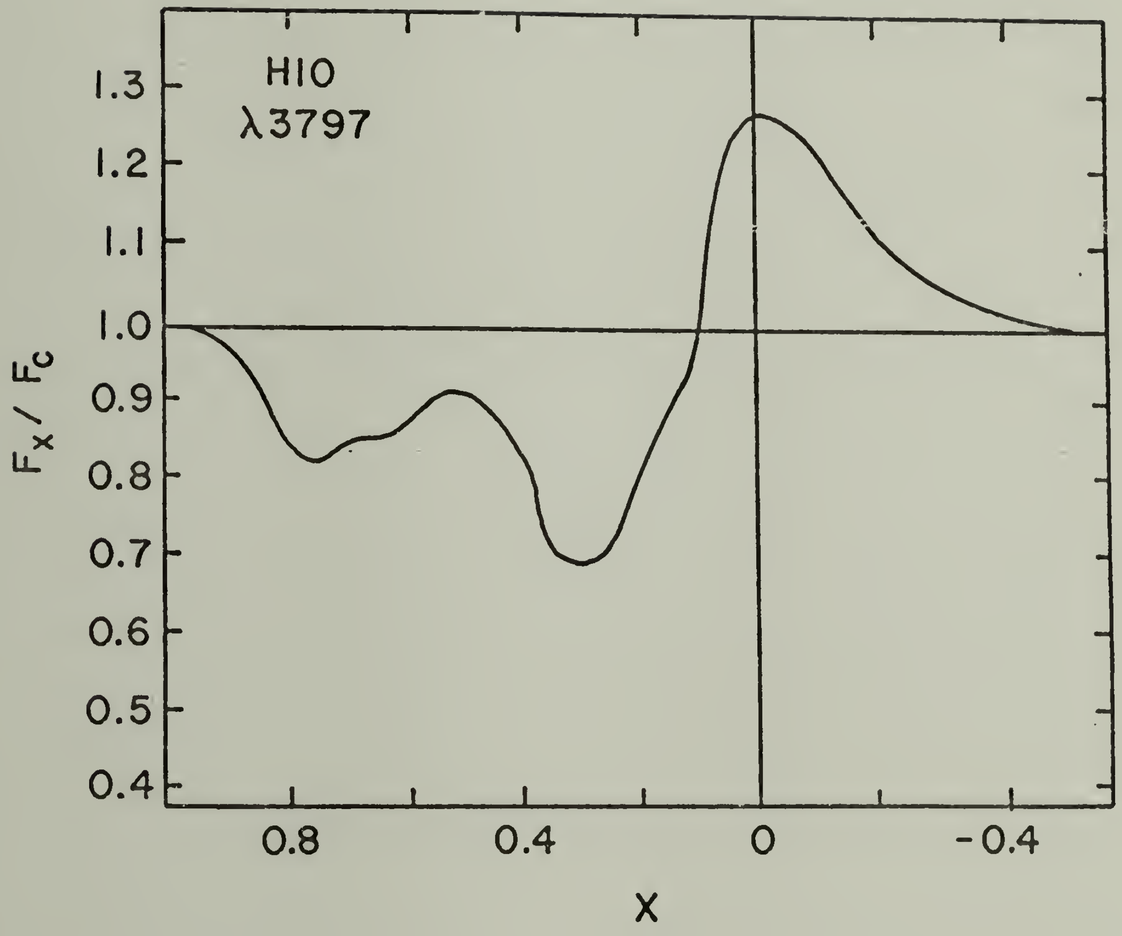
H10
λ3797
1.3
1.2
1.1
1.0
0.9
0.8
0.7
0.6
0.5
0.4
F_x / F_c
0.8
0.4
0
-0.4
X

shells in the envelope. However, a shell moving at ∿ 100 km s^{-1} (and probably expanding at near its thermal velocity) could not give rise to an absorption feature for more than a month or so. In fact, spectrograms taken at Mount Wilson show that the duplicity of absorption components observed in Hγ and Hδ in July 1942 has disappeared by late October of the same year. Therefore, the multiple absorption features seem to be transient phenomena and could be caused by moving shells in the envelope. On the other hand, the multiple absorption features may persist too long to be caused by shells in the atmosphere.

An accelerating flow can give rise to absorption features close to line center (because the optical depth is large near the star) whereas a decelerating envelope will always give an absorption feature with a larger violet displacement (because the central emission is usually too strong for an absorption feature to be formed near line center). These facts prompt the following question: Could the double absorption features just be a consequence of line formation in an envelope where the velocity of the flow first increases and then decreases? Kuan and Kuhi (1975) have already shown that it is quite easy to reproduce the early Balmer lines (Hα, Hβ, Hγ) using a decelerating flow. However, they point out that there must be a region near the photosphere where the atmosphere is accelerated to the escape velocity. This type of "ejected" flow probably occurs in many stars and galaxies, and so an investigation of line formation in this type of flow might be very rewarding.

The exact treatment of the transfer of radiation in an envelope that accelerates and then decelerates would be a monumental problem. Therefore, the reader should bear in mind that the following formulation is an approximate treatment of the radiation transfer.

Consider a star of radius R_* ejecting mass into an envelope of extent R_{max}. The gas accelerates outward to a radius R_c, and then decelerates. The velocity law to be used is a combination of equation (2) for the inner region, and the decelerating law used by Kuan and Kuhi for the outer region:

$$\begin{aligned} v(r \leq R_c) &= v_o(1 - R_*/r)^{1/2} \quad , \\ v(r \geq R_c) &= v_{max}(R_c/r)^{1/2} \quad . \end{aligned} \tag{38}$$

Matching the two velocity laws at $r = R_c$ gives the relation between v_o and v_{max}:

$$v_o = v_{max}(1 - R_*/R_c)^{-1/2} \quad . \tag{39}$$

In order to determine the appearance of the constant line of sight velocity surfaces, we must find the relation between r, p, and x. The dimensionless frequency parameter, x, is defined as $x = \mu v/v_{max}$. Using equation (39), this may be written as

$$x = \mu[(1 - R_*/r)/(1 - R_*/R_c)]^{1/2} \quad . \tag{40}$$

In order to find the minimum value of the radius for any given velocity surface, set $\mu = 1$ in equation (40) to give

$$r_{min} = R_*[1 - x^2(1 - R_*/R_c)]^{-1} \quad . \tag{41}$$

Since the outer portion of the envelope is decelerating, the velocity surfaces will be closed. Therefore, for a given value of p and x, there are two possible values of the radius r for which the line of sight velocity, v_z, is the same. Using equations (3) and (40), we have for $r < R_c$,

$$r^2[1 - x^2(1 - R_*/R_c)/(1 - R_*/r)] - p^2 = 0 \quad , \tag{42}$$

and for $r > R_c$

$$r^2[1 - x^2 r/R_c] - p^2 = 0 \quad . \tag{43}$$

Designating the value of p when the velocity law changes from accelerating to decelerating as p_c, we find from equation (42) that $p_c = R_c(1-x^2)^{1/2}$. So, for a given value of p and x, if $p < p_c$ then equation (42) gives the value of the radius on the velocity surface in the accelerating region, and equation (43) gives the radius in the decelerating region. If $p > p_c$, both roots are in the decelerating region and are given by equation (43). The constant line of sight velocity surfaces are completely determined by equations (42) and (43), and are shown in Figure 11. Notice that unlike the velocity surfaces for an accelerating atmosphere, all the surfaces pass through the region between the surface of the star and R_c.

As can been seen from Figure 11, for a given velocity surface, there is a maximum value of p. In order to find p_{max} and the radius to this point, we evaluate

$$\frac{\partial v_z}{\partial z} = \frac{\partial}{\partial z}\left(\mu \frac{v}{v_{max}}\right) = 0 \quad , \tag{44}$$

which after some algebra gives

$$p_{max} = \frac{2R_c}{3\sqrt{3}\, x^2} \quad , \tag{45}$$

and

$$r(p_{max}) = \frac{2R_c}{3x^2} \quad .$$

We can now write down the approximate equations for the line pro-

Figure 11: Constant line of sight velocity surfaces for a flow that accelerates out to a radius R_c, and then decelerates.

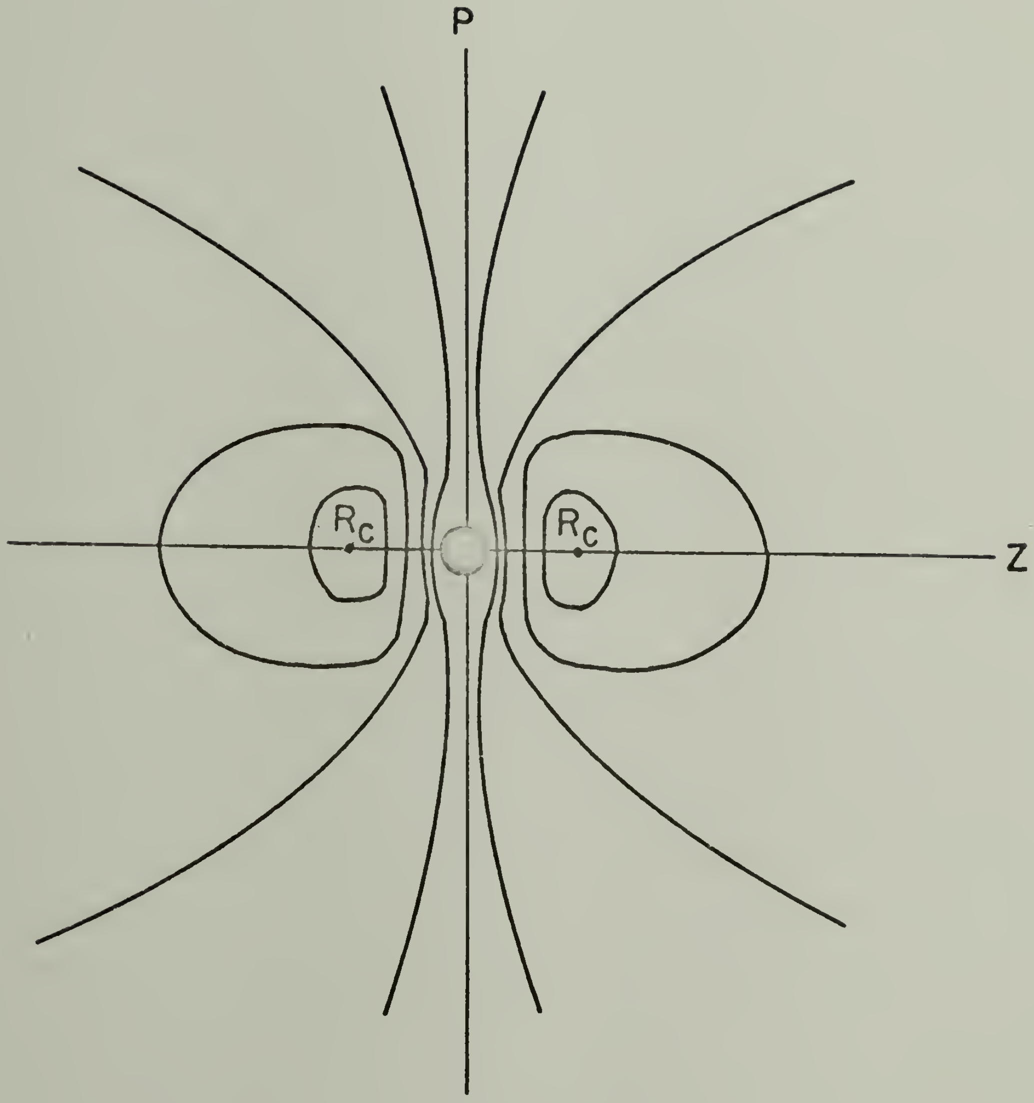
P
R_c
R_c
Z

files (for $x > 0$, $x < 0$, $p > R_*$, and $p < R_*$). In general, the flux can be written (Castor 1970):

$$\frac{F_x - F_c}{F_c} = F_e - F_a - F_o \quad , \tag{46}$$

where F_e is the emitted flux, F_a is the flux absorbed in the line, and F_o is the flux occulted by the star. On the blue side of the line ($x > 0$), there is no occultation. So, for $x > 0$ and $p_{max} \geq 1$ (in units of $R_* = 1$) we have

$$\frac{F_x - F_c}{F_c} = F_e - F_a = \int_{r_{min}}^{r_{max}} \frac{S(r)}{I_*} \frac{(1 - e^{-\tau(r)})}{\tau(r)} \tau_o(r) e^{-\tau(r)} \, 2rdr$$
$$- \int_0^1 \frac{I_*}{I_*} (1 - e^{-\tau(r)}) 2pdp \quad . \tag{47}$$

The emission integral must be broken into two parts because a photon must cross two constant velocity surfaces. Therefore, for $x > 0$, $p_{max} \geq 1$ we have

$$\frac{F_x}{F_c} = \int_{r_{min}}^{r(p_{max})} \frac{S(r)}{I_*} \frac{(1 - e^{-\tau_1})}{\tau_1} \tau_{o_1} \, e^{-\tau_2} \, 2rdr$$
$$+ \int_{r(p_{max})}^{R_{max}} \frac{S(r)}{I_*} \frac{(1 - e^{-\tau_2})}{\tau_2} \tau_{o_2} \, 2rdr$$
$$+ \int_0^1 \exp[-(\tau_1 + \tau_2)] 2pdp \quad . \tag{48}$$

In this equation, τ_1 and τ_2 are the optical depths at the inner and outer roots, respectively. The approximation made was in multiplying the first integrand in equation (48) by $e^{-\tau_2}$ to take into account the passage of the photon through the outer portion of the velocity surface.

Similarly, for $x > 0$ and $p_{max} < 1$, we have

$$\frac{F_x}{F_c} = \int_{r_{min}}^{r(p_{max})} \frac{S(r)}{I_*} \frac{(1 - e^{-\tau_1})}{\tau_1} \tau_{o_1} e^{-\tau_2} 2rdr$$

$$+ \int_{r(p_{max})}^{R_{max}} \frac{S(r)}{I_*} \frac{(1 - e^{-\tau_2})}{\tau_2} \tau_{o_2} 2rdr$$

$$+ \int_{o}^{p_{max}} \exp[-(\tau_1 + \tau_2)]\, 2pdp + \int_{p_{max}}^{1} 2pdp \quad , \tag{49}$$

the last term of which reduces simply to $(1 - p_{max}^2)$. For $x < 0$ and $p_{max} \leq 1$, the whole velocity surface is occulted by the star and we therefore have $F_x/F_c = 1$. For $x < 0$ and $p_{max} > 1$, we have

$$\frac{F_x}{F_c} = 1 + \int_{r_i(p=1)}^{r(p_{max})} \frac{S(r)}{I_*} \frac{(1 - e^{-\tau_1})}{\tau_1} \tau_{o_1} 2rdr$$

$$+ \int_{r(p_{max})}^{r_o(p=1)} \frac{S(r)}{I_*} \frac{(1 - e^{-\tau_2})}{\tau_2} \tau_{o_2} e^{-\tau_1} 2rdr \quad , \tag{50}$$

where $r_i(p=1)$ and $r_o(p=1)$ are the radii of the two points on the constant velocity surface where $p=1$.

The non-LTE source functions and optical depths in the lines for hydrogen were calculated for this "ejected" flow using the escape probability method. These values were then used in the equations derived above to compute the line profiles. The line profile program was tested in two limits: (1) $R_c = R_*$ (a simple decelerating envelope) and (2) $R_c = \infty$ (a simple accelerating envelope). For case (1), the program produced a line profile for Hα almost identical to the profile derived by Kuan and Kuhi (1975) for a simple decelerating envelope. The profile pro-

Figure 12: Theoretical line profiles for Balmer 10 obtained from an envelope that accelerates and then decelerates. The three different profiles correspond to the three different values of R_c as shown in the figure.

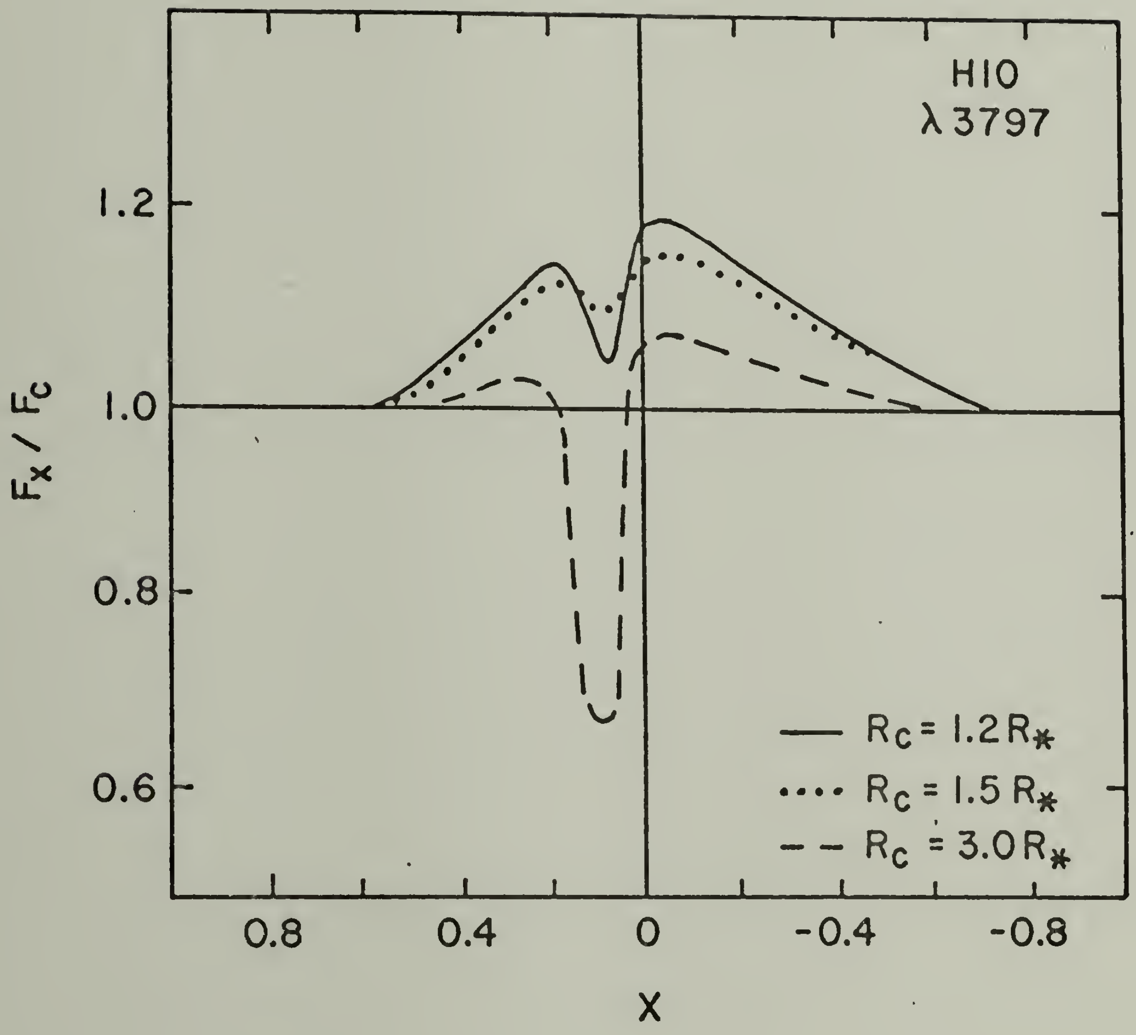
H10
λ3797
1.2
1.0
0.8
0.6
F_x / F_c
0.8
0.4
0
-0.4
-0.8
X
$R_c = 1.2 R_*$
$R_c = 1.5 R_*$
$R_c = 3.0 R_*$

duced by using case (2) was also the same as that using a tested line profile program for an accelerating flow. Therefore, the numerical evaluation of the integrals in equations (48) - (50) was accurate.

The line profile for λ3797 (H10) was then computed for the three cases $R_c = 1.2\ R_*$, $1.5\ R_*$, and $3.0\ R_*$. The results are shown in Figure 12. Clearly no double absorption features are present, but the profiles are quite unusual in appearance. The mutilation of the emission on the shortward side of the line is caused by absorption very close to the star. H10 is very weak and the optical depth in the line decreases rapidly with radius. The fact that there is virtually no absorption beyond $x \approx .2$ results in the unusual behavior of the flux rising above the continuum on the blue side of the absorption component.

There exists at least one P Cygni star that exhibits this type of unusual line profile. The Hβ line of MWC 342 has a very narrow central emission and an absorption feature on the shortward side that dips sharply to a point a little below the continuum and then rises back up to a level twice that of the continuum at $x \sim .5$.

In conclusion, it appears that this type of "ejected" flow will not produce multiple absorption components in P Cygni profiles, and we are left to speculate about the presence of shells in the atmosphere.

The Early Balmer Lines

Even though a rapidly accelerating envelope is able to produce the weak HeI lines, it cannot produce the strong Balmer lines of hydrogen, as previously mentioned. If the gas is accelerating, it must be doing so at a much slower rate than in the velocity law used for the HeI model.

The velocity law inferred from the infrared free-free spectrum by Barlow and Cohen (1977) is also a slowly accelerating one. Therefore, in this section, we will investigate the Balmer line profiles produced by a stellar wind which has a velocity that increases linearly with distance from the star (see equation (13)).

Before building a detailed model, let us investigate in more detail why it is difficult to produce the early Balmer lines with an accelerating flow. This can be shown quite easily from the expression for the emitted flux in the line (Castor 1970):

$$F_e = \frac{1}{R_*^2} \int_{r_{min}}^{\infty} \frac{S(r)}{I_*} \frac{(1 - \exp(-\tau(r)))}{\tau(r)} \tau_o(r)\, 2r dr \quad . \tag{51}$$

Let us assume a velocity law of the form $v = v_o r/R_*$. Since this velocity law has no terminal velocity, we must replace the upper limit of the above integral with r_{max} instead of infinity. In order to simplify the integral, assume that the source function is constant over the emitting volume and that the optical depth is everywhere much greater than unity. The integral becomes

$$F_e = \frac{2\bar{S}}{R_*^2 I_*} \int_{r_{min}}^{r_{max}} r(1 + \sigma\mu^2) dr \quad . \tag{52}$$

For the velocity law $v = v_o r/R_*$, we have $\sigma = 0$ and $r_{min} = x r_{max}$ (see Chapter II). The emitted flux becomes

$$F_e = \frac{\bar{S}}{I_*} \left(\frac{r_{max}}{R_*}\right)^2 (1 - x^2) \quad . \tag{53}$$

Written in this manner, it is easy to see that the emission has a parabolic shape and is positive everywhere except at $|x| = 1$, where it vanishes. In order to produce an absorption component at a frequency displacement x, we must have $F_a > F_e$, where F_a is the absorbed flux (see equation (46)). If the central intensity of the emission component is, say, twelve times the continuum, then the approximate form of the emitted flux is $F_e \approx 12(1 - x^2)$. At a frequency displacement $x = .8$, we have $F_e = 4.32$. Since the absorbed flux has the limits $0 \leq F_a \leq 1$, $F_a < F_e$ and an absorption component will not be present. In deriving equation (53), the only assumptions made were that the optical depth was everywhere large and that the source function was constant over the emitting region. The former assumption should be rather good (in fact it is required in order to get a deep absorption). So, it appears that the only way in which the Balmer lines can be produced in an accelerating flow is if the source function is not constant but decreases rapidly with radius. The emission component would no longer be parabolic and would be small enough in the wings for an absorption feature to be formed.

The radial dependence of the source function for Balmer alpha can be investigated by using a simple three level atom. Using equation (26), the net rate by which level three is populated can be written in the form

$$\frac{dN_3}{dt} = 0 = -N_3A_{32}\beta_{32} - N_3A_{31}\beta_{31}$$

$$+ (N_2B_{23} - N_3B_{32})\beta_{32}WI_{*32} + (N_1B_{13} - N_3B_{31})\beta_{31}WI_{*31}$$

$$+ N_e^2\alpha_3 - N_3P_3 \quad , \tag{54}$$

where W is the dilution factor and P_3 is the photoionization rate out of level three, where in general we have (approximately)

$$P_n = 4\pi W \int_{\nu_n}^{\infty} \frac{B_\nu(T_*)}{h\nu} a_\nu(n) d\nu \quad . \tag{55}$$

Similarly, the net rate by which level two is populated is given by

$$\frac{dN_2}{dt} = 0 = -N_2A_{21}\beta_{21} + (N_1B_{12} - N_2B_{21})W\beta_{21}I_{*_{21}} + N_3A_{32}\beta_{32}$$
$$+ (N_3B_{32} - N_2B_{23})W\beta_{32}I_{*_{32}} + N_e^2\alpha_2 - N_2P_2 \quad . \tag{56}$$

In equations (54) and (56), the collision rates have been omitted since they have a negligible effect on the level populations (Mihalas 1970). In order to produce the deep absorption in Hα, we consider the case where $\tau_{32} > 1$ over most of the envelope. This in turn implies that the optical depths in Lyα and Lyβ will be very large. In this limit, β_{21} and β_{31} are negligible, and for simplicity we set them equal to zero. Equations (54) and (56) reduce to

$$-N_3A_{32}\beta_{32} + (N_2B_{23} - N_3B_{32})W\beta_{32}I_{*_{32}} + N_e^2\alpha_3 - N_3P_3 = 0 \quad , \tag{57a}$$

$$N_3A_{32}\beta_{32} + (N_3B_{32} - N_2B_{23})W\beta_{32}I_{*_{32}} + N_e^2\alpha_2 - N_2P_2 = 0 \quad . \tag{57b}$$

Adding these two equations gives the condition

$$N_e^2\alpha_2 - N_2P_2 = -N_e^2\alpha_3 + N_3P_3 \quad . \tag{58}$$

Now, the source function in Hα, S_{32}, is related to the populations of levels two and three by the equation, $S_{32} = N_3A_{32}/(N_2B_{23} - N_3B_{32})$. Using this relation we can write the population of level two in terms of N_3 and S_{32}. This expression for N_2 can then be substituted into equation (58) to give

$$N_3 = \frac{N_e^2(\alpha_2+\alpha_3)}{(P_3+P_2(\frac{A_{32}}{B_{23}S_{32}}+\frac{B_{32}}{B_{23}}))} \quad . \tag{59}$$

Now, dividing equation (57a) through by $(N_2B_{23}-N_3B_{32})\beta_{32}$ gives

$$0 = -S_{32} + WI_{*_{32}} + \frac{N_e^2\alpha_3}{(N_2B_{23}-N_3B_{32})\beta_{32}} - \frac{S_{32}}{A_{32}}\frac{P_3}{\beta_{32}} \quad . \tag{60}$$

Combining terms in this equation, eliminating N_3 by the use of equation (59), and solving for the source function gives (after some tedious algebra)

$$S_{32} = \frac{[\beta_{32}WI_{*_{32}} + \frac{P_2}{B_{23}}(\frac{\alpha_3}{\alpha_2+\alpha_3})]}{[\beta_{32} - (\frac{\alpha_3}{\alpha_2+\alpha_3})\frac{B_{32}}{B_{23}A_{32}}P_2 + (\frac{\alpha_2}{\alpha_2+\alpha_3})\frac{P_3}{A_{32}}]} \quad . \tag{61}$$

So, now we have expressed the source function for Hα in terms of atomic constants, the dilution factor, and the escape probability in the Hα line. From equation (55) we see that $P_n \propto W$. Therefore, the source function can be written in the form

$$S_{32} = \frac{a\beta_{32} + b}{(\frac{\beta_{32}}{W} + c)} \quad , \tag{62}$$

where a, b, and c are constants independent of radius given by (assuming $T_* = 2 \times 10^4$ K):

$$a = I_{*_{32}} = 7 \times 10^{-4}$$

$$b = \frac{1}{B_{23}} \left(\frac{\alpha_3}{\alpha_2 + \alpha_3}\right)\left(\frac{P_2}{W}\right) = 7.7 \times 10^{-5}$$

$$c = -\frac{B_{32}}{B_{23}} \left(\frac{\alpha_3}{\alpha_2 + \alpha_3}\right) \frac{1}{A_{32}} \left(\frac{P_2}{W}\right) + \frac{1}{A_{32}} \left(\frac{\alpha_2}{\alpha_2 + \alpha_3}\right)\left(\frac{P_3}{W}\right) = 0.1 \quad . \qquad (63)$$

Near the star, the optical depth in Hα is very large (on the order of 10^5), and, therefore, $\beta_{32} \approx 1/\tau_{32} \sim 10^{-5}$. From equation (62), we can see that since β_{32} is so small, S_{32} is governed by the value of the constants b and c. At $r \approx R_*$, we find that $S_{32} \approx 7 \times 10^{-4} \approx I_{*_{32}}$. The source function in Hα does not start to decrease rapidly until β_{32} has increased to a value of ~ 0.1 and $r \gtrsim 10R_*$. At these radii, the radial dependence of S_{32}, to a good approximation, is given by

$$S_{32} = W(a + b/\beta_{32}) \quad . \qquad (64)$$

As the radius increases, β_{32} approaches an upper limit of unity, and therefore the source function in Hα can decrease with radius very rapidly.

Under the assumptions made above (optical depth in the Lyman lines infinite, $\tau_{32} > 1$, validity of using a three level atom), we find that the source function in Hα can decrease almost as fast as the dilution factor. In order to produce a deep absorption in the violet wing of Hα, the source function does not have to decrease with radius quite this rapidly. However, if our simple analytic treatment showed that the source function could not decrease rapidly with radius, the accelerating envelope hypothesis would be in severe trouble.

In order to calculate the accurate radial dependence of the source functions for the Balmer lines, the statistical equilibrium equations for a multilevel atom must be solved. Therefore, a detailed model for neutral hydrogen emission in P Cygni's envelope was constructed assuming that the velocity of the flow increases linearly with distance from the star. Once the velocity law is stipulated, there are four parameters that affect the line profiles that need to be chosen: (1) the velocity of the flow at the surface of the star, v_o, (2) the stellar temperature, T_*, (3) the maximum velocity of outflow, v_{max}, and (4) the mass loss rate of the star, $\dot{M}$. The velocity of the flow at R_* is most likely equal to the thermal velocity of a gas at the temperature T_*, e.g. $v_o = 12.85 (T_*/10^4)^{1/2}$ kms^{-1}. However, the actual value of v_o could be somewhat different than this. Likewise, we do not know exactly what the maximum outflow velocity is, but we will continue to use the value of 280 kms^{-1} suggested by Kuan and Kuhi (1975). A more accurate determination of P Cygni's radius and temperature gives $R_* = 90\ R_\odot$ and $T_* \approx 20{,}000$ K (Barlow and Cohen 1977), and these values will be used in this model. Therefore, v_o, v_{max}, T_*, and R_* are more or less fixed so that really the only free parameter is the mass loss rate, $\dot{M}$.

The statistical equilibrium equations were set up for a twelve level neutral hydrogen atom and were solved at fifty points in the envelope. It was found that for the conditions in P Cygni's envelope, using only six levels gave the same source function for Hα as using twelve levels. Therefore, the populations of the lower levels are not really affected by recombination and cascade from levels greater than ∿ 6.

The solution of the equilibrium equations was carried out in the same manner as described previously, except for the treatment of the diffuse radiation field. The populations of the levels are dominated by photoionizations, recombinations and radiative transitions between the various levels. Since the line profile of Hα depends crucially on the radial dependence of the line source function, the radial dependence of the populations of the second and third levels needs to be calculated as accurately as possible. A more accurate method of treating the diffuse radition field is to invoke the on-the-spot (OTS) approximation. The OTS approximation amounts to assuming that diffuse ionizing photons will be absorbed close to the point at which they are generated. Therefore, recombinations to the ground state will be balanced by diffuse photoionizations.

The OTS approximation is fairly accurate in an optically thick nebula, except near a boundary. The approximation breaks down near a boundary because a diffuse ionizing photon is not really absorbed at its point of emission, but will travel roughly one mean free path before being absorbed. The mean free path of a photon of wavelength $\lambda = 912\text{Å}$ is

$$\ell = (N(HI)a_{\nu_o})^{-1} \quad , \tag{65}$$

where N(HI) is the density of neutral hydrogen and a_{ν_o} is the photoionization cross section of hydrogen at the Lyman edge. The approximate density of neutral hydrogen can be calculated in the following manner. The ratio of the number of ionized hydrogen atoms to the number of neutral atoms is given by

$$\frac{N(HII)}{N(HI)} = 4\pi(N_e\alpha_B)^{-1} \int_{\nu_o}^{\infty} \frac{J_\nu}{h\nu} a_\nu d\nu \quad , \tag{66}$$

where J_ν is the mean intensity of the stellar radiation field, and α_B

is the case B recombination coefficient. Assuming $J_\nu = B_\nu(T_*)$, where $B_\nu(T_*)$ is the Planck function, we have

$$\frac{N(HII)}{N(HI)} = 8\pi a_{\nu_o} \nu_o{}^3 (N_e \alpha_B c^2)^{-1} \int_{\nu_o}^{\infty} \frac{d\nu}{\nu} \left[\exp\left(\frac{h\nu}{kT_*}\right) - 1\right]^{-1} , \qquad (67)$$

where $a_\nu = a_{\nu_o} (\nu_o/\nu)^3$. For $T_* = 20{,}000$ K, $\alpha_B = 1.43 \times 10^{-13}$ cm^3 s^{-1} and the integral in equation (67) is approximately equal to 4×10^{-5}. Using an appropriate value for the electron density for a mass loss rate of 1.5×10^{-5} $M_\odot$yr^{-1} gives $N(HII)/N(HI) \approx 3 \times 10^6$. Now, using the additional fact, $N(HI) + N(HII) = N_H$, we find $N(HI) \approx 10^5$ cm^{-3}. Equation (65) for the mean free path then gives $\ell \approx 1R_*$ where $R_* = 90R_\odot$. Therefore, a diffuse ionizing photon emitted within $1R_*$ of the stellar surface has a good chance of escaping from the envelope by penetrating the stellar photosphere. Beyond $\sim 2R_*$, the diffuse photon will probably be absorbed in the surrounding media and so the OTS approximation is valid.

Assuming that photons are emitted isotropically, a photon emitted just outside the star's surface will have roughly a 50% chance of escaping the envelope and a 50% chance of being absorbed. Let γ be the factor by which the number of recombinations to the ground state resulting in a diffuse ionizing photon exceeds the number of diffuse photoionizations. At $r = R_*$ we have $\gamma \approx 2$, and for $r \geq 2R_*$, $\gamma \approx 1$. Therefore, γ is a decreasing function of radius, and, for simplicity, we will assume that γ decreases linearly with distance from the star.

Using this method to treat the diffuse radiation, the statistical equilibrium equations were solved and the line profiles were calculated for the velocity law $v = v_o r/R_*$. The resulting profiles for Hα, Hβ, and $H\gamma$ are shown in Figures 13, 14, and 15, along with the observed lines and the profiles computed by Kuan and Kuhi (1975) for a decelerating flow. The parameters used are $v_0 = 18$ km s^{-1}, $v_{max} = 280$ km s^{-1}, and $\dot{M} = 1.5 \times 10^{-5}\ M_\odot yr^{-1}$. By varying these parameters, the profiles can be changed somewhat but not enough to give a significantly better profile.

A quick look at the calculated profiles shows that this model does not have any trouble producing a large central intensity. However, the model does not allow us to produce an arbitrarily deep absorption component. If the mass loss rate is increased much more than the value used here, the emission component becomes too large. If $\dot{M}$ is decreased, the emission component will be smaller, but then the optical depth in the wings of the line will be too small, e.g. there will not be any absorption in the blue wing.

The fact that this model produces Balmer lines with violet displaced absorption components indicates that the source functions in the lines are decreasing rapidly with radius. However, the source functions for the early Balmer lines are not decreasing rapidly enough to give a really deep absorption. The source function in $H\alpha$ is related to the level populations by $S_{32} \propto (g_3N_2/(g_2N_3) - 1)^{-1}$. In order for S_{32} to decrease rapidly with radius, the ratio N_2/N_3 must increase rapidly with radius. This fact implies an optically thin Balmer continuum. Otherwise, photoionizations out of level two would make it difficult for the ratio N_2/N_3 to increase rapidly. For the model presented here, with $\dot{M} = 1.5 \times 10^{-5}\ M_\odot yr^{-1}$, the optical depth at the Balmer edge at $r \approx 15R_*$ is only ~ 0.1. Therefore, the second level is not becoming depopulated by photoionizations, and if the velocity law $v \propto r$ is roughly correct, then some unknown mechanism

Figure 13: Line profile for Hα. The solid curve is the theoretical profile obtained by using the velocity law $v = v_o r/R_*$ and $\dot{M} = 1.5 \times 10^{-5}\ M_\odot yr^{-1}$. The dashed curve is the observed profile, and the dotted curve is the profile computed by Kuan and Kuhi (1975) using a decelerating atmosphere.

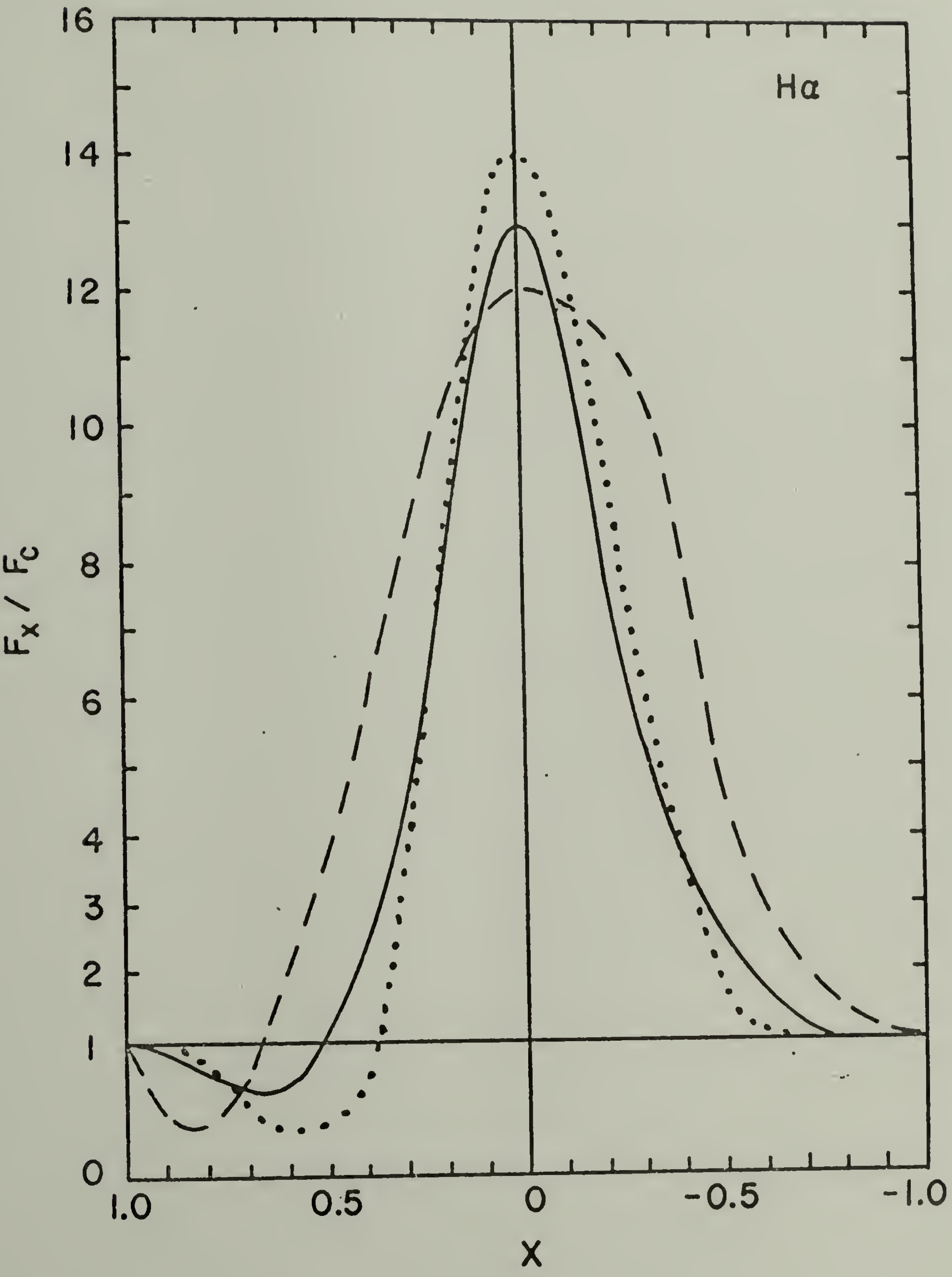
Hα
F_x / F_c
16
14
12
10
8
6
4
3
2
1
0
1.0
0.5
0
-0.5
-1.0
X

Figure 14: Line profile for Hβ. The solid curve is the theoretical profile obtained by using the velocity law $v = v_o r/R_*$ and $\dot{M} = 1.5 \times 10^{-5}\ M_\odot yr^{-1}$. The dashed curve is the observed profile, and the dotted curve is the profile computed by Kuan and Kuhi (1975) using a decelerating atmosphere.

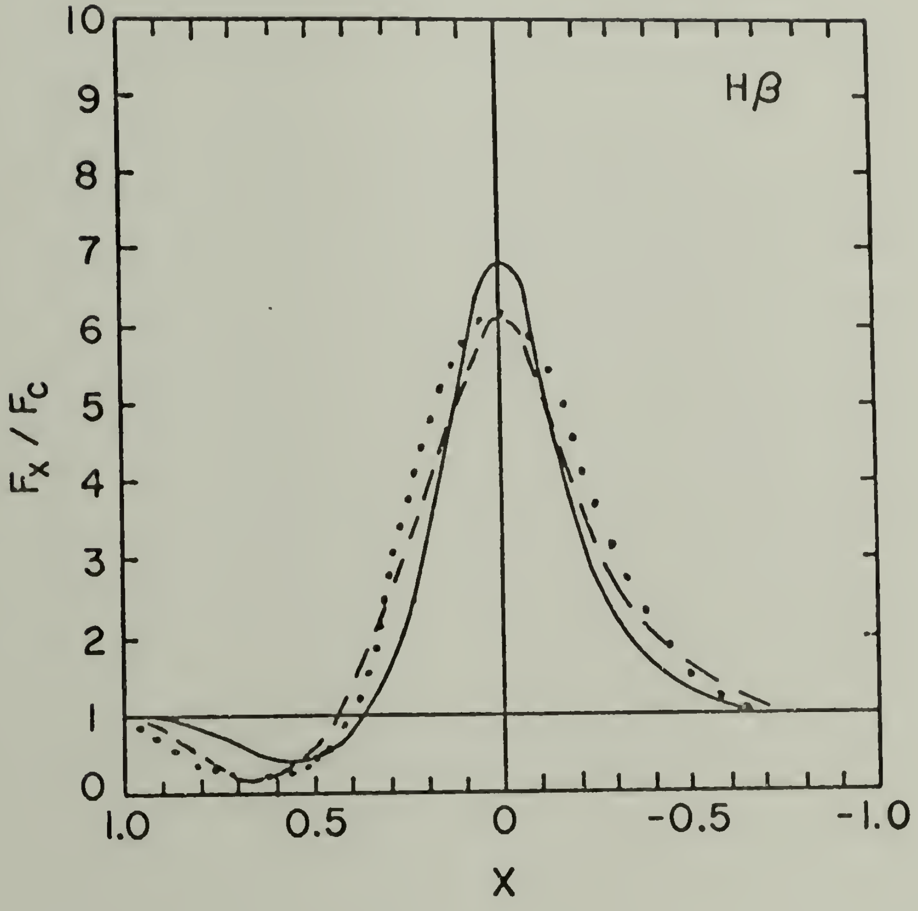
Hβ
F_x / F_c
X
10
9
8
7
6
5
4
3
2
1
0
1.0
0.5
0
-0.5
-1.0

Figure 15: Line profile for Hγ. The solid curve is the theoretical profile obtained by using the velocity law $v = v_o r/R_*$ and $\dot{M} = 1.5 \times 10^{-5}\ M_\odot yr^{-1}$. The dashed curve is the observed profile, and the dotted curve is the profile computed by Kuan and Kuhi (1975) using a decelerating atmosphere.

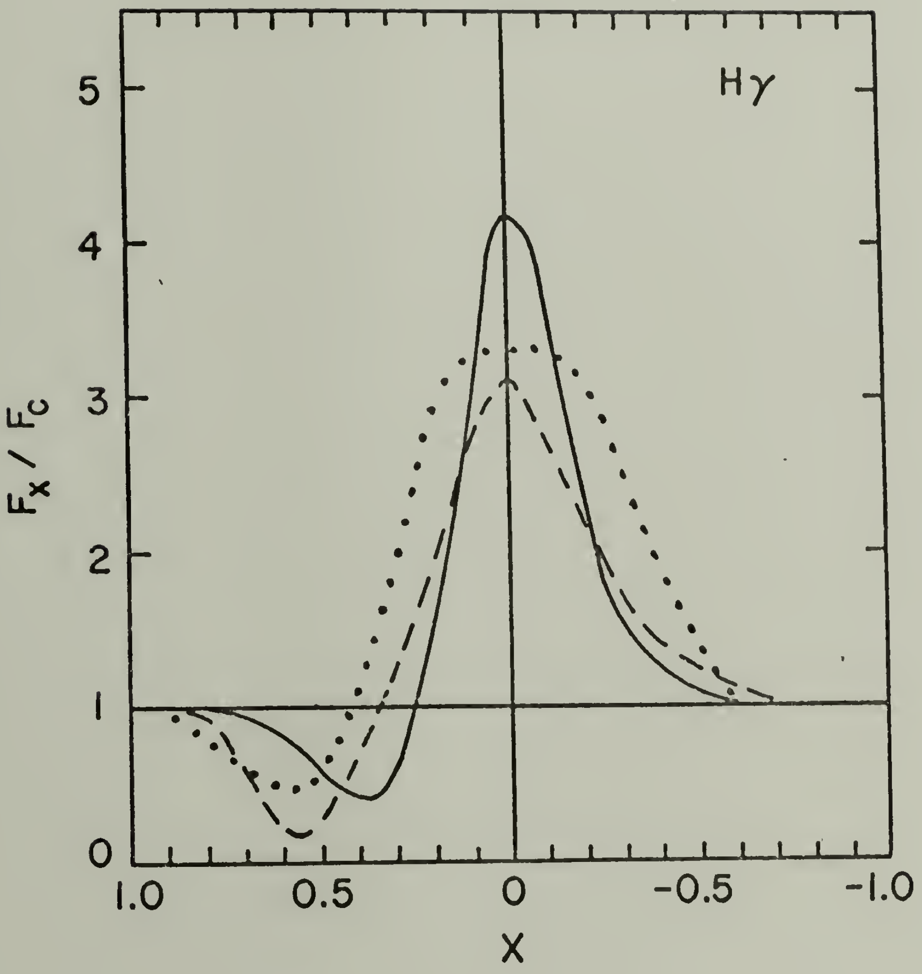
Hγ
5
4
3
2
1
0
F_x / F_c
1.0
0.5
0
-0.5
-1.0
X

must be operating to overpopulate level two.

In order to explain P Cygni's infrared spectrum, Barlow and Cohen (1977) derived a slowly accelerating velocity law. The velocity increases roughly linearly with radius out to $\sim 8R_*$, beyond which the velocity increases very slowly, resulting in a very extended envelope. It is very difficult, if not impossible, to produce a deep absorption in the early Balmer lines with this type of flow, because the envelope will become optically thin at small frequency displacements.

The velocity law $v \propto r$ has no terminal velocity in the flow. To circumvent this problem, we defined a maximum velocity of outflow, v_{max}, which is attained at a radius $r_{max} = R_* v_{max}/v_o$. In doing this, we actually ignored any contribution to the line profile arising in the envelope at radii greater than r_{max}. Strictly speaking, this is valid only if the optical depth in the line is equal to zero beyond r_{max}, because there will be no additional absorption or emission in the line (see equation (51)). In most of the models that were computed, at $r = r_{max}$, $\tau(H\alpha) \lesssim 1$, and $\tau(H\alpha)$ approaches zero rapidly for $r > r_{max}$. This fact, coupled with the rapid decrease of the source function with radius, allows us to ignore contributions to the line from $r > r_{max}$ without incurring too much error. Including contributions to the line from radii greater than r_{max} will increase the emission component at line center only slightly and will make the absorption component somewhat shallower. Since this model does have a problem in producing a deep absorption anyway, the latter point is the most serious objection to truncating the envelope at $r = r_{max}$.

Discussion of Results

The evidence presented in this chapter strongly indicates that the gas in P Cygni's circumstellar envelope is slowly accelerating. The simple velocity law, $v \propto r$, used to model the early Balmer lines in the previous section, is probably not a bad representation of the actual flow. This result is very interesting in view of the present predictions of stellar wind theory. The theory of radiation-driven mass loss of Of stars formulated by Castor, Abbott, and Klein (1975), (hereafter referred to as CAK), predicts a rapidly increasing velocity flow in the supersonic region. The equations governing the flow are of mass conservation

$$\dot{M} = 4\pi r^2 \rho v = \text{constant} \quad , \qquad (68)$$

and of momentum balance

$$v \frac{dv}{dr} + \frac{1}{\rho} \frac{dP_g}{dr} + \frac{GM_*}{r^2} [1 - \Gamma] = 0 \quad , \qquad (69)$$

where ρ is the mass density, P_g is the gas pressure, M_* is the stellar mass and Γ is defined as

$$\Gamma = (\gamma + 1) \frac{\sigma_e L_*}{4\pi G M_* c} \quad , \qquad (70)$$

where L_* is the stellar luminosity and σ_e is the mass scattering coefficient of the free electrons. Physically speaking, Γ is the ratio of the total radiation force on the gas to the gravitational force, and γ, the force multiplier, is the ratio of the force in the lines to the force in the continuum.

CAK found that the inclusion of a great number of subordinate lines made important contributions to the total radiation force. Furthermore, they found that the supersonic region is characterized by an almost constant value of $\gamma > 1$. This means that equation (69) can be integrated to give the velocity law

$$v(r) = v_\infty(1 - r_s/r)^{1/2} \quad , \tag{71}$$

in the supersonic region, where the sonic radius, r_s, is essentially the same as the photospheric radius, R_*. Therefore, the very detailed analysis of radiation pressure in the lines by CAK results in the same rapidly accelerating velocity law that has been used (without any real justification) for line profile calculations (Castor 1970, Van Blerkom 1973).

Even though P Cygni is losing mass at a tremendous rate, we must be careful in comparing the stellar wind theory of CAK to our results. CAK considered the radiation pressure in the lines of only one ion, CIII. This ion is fairly abundant in the envelopes of O type stars, but its presence in the atmosphere of P Cygni (Blp) has not been confirmed (de Groot 1969). Even if it is present, the fraction of doubly ionized carbon atoms is probably small because of P Cygni's low temperature (∿ 20,000 K). Besides, P Cygni is not a normal star and it would be somewhat presumptuous to infer from our results that the stellar wind theory of CAK is incorrect. The differences may indicate something unusual about the mode of mass loss operating in P Cygni.

It should be pointed out here that the presence of a slowly accelerating flow in P Cygni's envelope does not invalidate the explanation given previously of the different violet displacements of absorption components in HeI lines of the same series. From equation (36) we have

$$\tau(x, p=0, z=\infty) \propto (f(r)/r^2 \; dv^2/dr)_{r_o} \quad , \tag{72}$$

where $f(r) = N_\ell/N_{He}$. Using the velocity law $v = v_o r/R_*$, we find that $\tau \propto f(r)r^{-3}$, and so the optical depth in a line decreases with increasing radius. Therefore, strong lines will have absorption components shifted further to the blue than weaker lines for the same reasons given previously.

CHAPTER V

SUMMARY

The physical conditions in the envelopes of MR 119 (a representative WN8 star) and P Cygni have been investigated by analyzing their emergent spectra. Using the escape probability method to simplify the transfer of radiation, models for P Cygni and MR 119, based on the HeI spectrum, were calculated.

Using a "one point" model for MR 119, the line intensities for HeI were computed and compared with the observations. It was found that at a distance of $3R_*$ from MR 119 the total helium density was $5\text{-}7 \times 10^{10}$ cm^{-3} and the temperature was ∿ 20,000K. This value of the density requires a mass loss rate of $\sim 10^{-4}\ M_\odot yr^{-1}$ from MR 119. This mass loss rate is comparable to the maximum rate expected from a Wolf-Rayet star.

Because recent interpretations of hydrogen emission lines in the envelope of P Cygni by de Groot (1969) and Kuan and Kuhi (1975) reached different conclusions, the HeI spectrum was investigated to see if a consistent model could be found. The statistical equilibrium equations were solved at several points in an accelerating envelope and the resulting run of source functions and optical depths were used to calculate line profiles. The calculated profiles agree quite well with the observed lines for a mass loss rate of $2 \times 10^{-6}\ M_\odot yr^{-1}$. The unusual behavior of the helium lines, in which absorption components of lines in the same series have quite different displacements from line center, is a natural consequence of the model. These results together with the evidence of the velocity-excitation potential relation strongly indicate an accelerating flow in the region where the neutral helium lines are formed.

An approximate method for dealing with the transfer of radiation in a flow that is accelerated and then decelerated was formulated in order to explain the double absorption components seen in many lines. However, the line profile for H10 ($10 \rightarrow 2$) produced in this type of flow did not possess the characteristic double absorption components displayed by the observed line.

A recent interpretation of the frequency dependence of the infrared flux from P Cygni indicates a slowly accelerating flow (Barlow and Cohen 1977). The early Balmer lines, which have large central intensities and deep absorption components, cannot be produced in a rapidly accelerating envelope. Therefore, a detailed model for HI emission in a slowly accelerating envelope ($v \propto r$) was constructed. The resultant line profiles of Hα, Hβ, and Hγ for a mass loss rate of 1.5×10^{-5} $M_\odot yr^{-1}$ agreed rather well with the observed profiles. This mass loss rate is larger than that found from the analysis of the HeI lines because a different radius was adopted in the two models. The calculated emission components of the Balmer lines were acceptable, but the violet shifted absorption components were not quite deep enough.

It was shown that the source function in a line must decrease rapidly with radius in order to produce a deep absorption. Using a three level atom, the radial dependence of the source function in Hα was derived, and it was found that under certain conditions the source function can decrease as fast as the dilution factor.

In conclusion, the evidence of the velocity-excitation potential relation, together with the interpretations of the infrared free-free spectrum and the model of the early Balmer lines constructed here, all point to a slowly accelerating flow in the circumstellar envelope of P Cygni. This result is very interesting because the present theory of radiation driven mass loss formulated by Castor, Abbott, and Klein (1975) predicts a rapidly increasing velocity in the supersonic region of the atmosphere.

REFERENCES

Adams, W. S. and Merrill, P. W. 1957, Ap. J. 125, 102.

Barlow, M. and Cohen, M. 1977, Ap. J. (in press).

Beals, C. S. 1929, M.N.R.A.S. 90, 202.

________. 1935, M.N.R.A.S. 95, 580.

________. 1938, Trans. I.A.U. 6, 248.

________. 1950, Pub. Dom. Ap. Obs. Victoria 9, 1.

Brocklehurst, M. 1971, M.N.R.A.S. 153, 474.

________. 1972, M.N.R.A.S. 157, 211.

Burgess, A. and Seaton, M. 1959, M.N.R.A.S. 120, 132.

Castor, J. I. 1970, M.N.R.A.S. 149, 111.

Castor, J. I. and Van Blerkom, D. J. 1970, Ap. J. 161, 485.

Castor, J. I., Abbott, D. C., and Klein, R. I. 1975, Ap. J. 195, 157.

de Groot, M. 1969, B.A.N.S. 20, 225.

Gordon, W. 1929, Ann. Phys. 2, 1031.

Green, L. C., Johnson, N. C., and Kolchin, E. K. 1966, Ap. J. 144, 369.

Griem, H. R. 1963, Phys. Rev. 131, 1170.

Kuan, P. and Kuhi, L. 1975, Ap. J. 199, 148.

Kuhi, L. V. 1968, NBS Spec. Pub. No. 307, p. 101.

Kuhi, L. V. and Smith, L. F. 1972, Atlas of Wolf-Rayet Line Profiles, unpublished.

Limber, D. N. 1964, Ap. J. 139, 1251.

Lucy, L. B. and Solomon, P. M. 1970, Ap. J. 159, 879.

Magalashvili, N. L. and Kharadze, E. K. 1967, Observatory 87, 295.

Mihalas, D. and Stone, M. 1968, Ap. J. 151, 293.

Mihalas, D. 1970, *Stellar Atmospheres* (W. H. Freeman and Co., San Francisco).

Morton, D. C. 1967, Ap. J. *147*, 1017.

————. 1968, *Mass Loss From Stars*, Springer-Verlag.

Paczynski, B. 1969, Acta Astronomica *17*, 355.

————. 1972, I.A.U. Symposium *49*, *Wolf-Rayet and High Temperature Stars*, ed. M. Bappu and J. Sahade, (Dordrecht: Reidel), p. 143.

Pengelly, R. M. and Seaton, M. J. 1964, M.N.R.A.S. *127*, 165.

Rublev, S. V. 1964, Astron. Zh. *41*, 1063.

Schwarzschild, M. and Härm, R. 1959, Ap. J. *129*, 637.

Simon, N. and Stothers, R. 1969, Ap. J. *155*, 247.

Smith, L. F. 1972, I.A.U. Symposium *49*, *Wolf-Rayet and High Temperature Stars*, ed. M. Bappu and J. Sahade (Dordrect: Reidel), p. 15.

Sobolev, V. V. 1960, *The Moving Envelopes of Stars* (Harvard University Press, Cambridge, Massachusetts).

Struve, O. 1935, Ap. J. *81*, 66.

Van Blerkom, D. J. 1972, I.A.U. Symposium *49*, *Wolf-Rayet and High Temperature Stars*, ed. M. Bappu and J. Sahade (Dordrecht: Reidel), p. 165.

APPENDIX

In this appendix, the necessary equations are presented for computing the atomic rates for bound-bound and bound free transitions of neutral helium.

Collisional Excitation Rates. The formulae used for collisional excitation rates are given by Mihalas and Stone (1968). In the transition $n'\ell' \rightarrow n\ell$, the collisional excitation rate is

$$C_{n\ell,n'\ell'} = CT^{1/2}[4f_{n\ell,n'\ell'}\left(\frac{E_H}{E_0}\right)^2]U_0[E_1(U_0) - \frac{U_0}{U_1}e^{-0.2}E_1(U_1)] \quad , \quad (A1)$$

where E_0 is the threshold energy of the transition, $f_{n\ell,n'\ell'}$ is the oscillator strength of the transition, and $C = 5.465 \times 10^{-11}$. E_H is the ionization potential of hydrogen, $U_0 = E_0/kT$, $U_1 = U_0 + 0.2$, and $E_1(x)$ is the exponential integral. For transitions between states with $\ell \leq 2$ (which are fairly nonhydrogenic), the oscillator strengths given by Green, Johnson, and Kolchin (1966) were used. For $\ell \geq 3$, the oscillator strengths were calculated from the spontaneous transition probabilities.

Collisional Ionization Rate. The appropriate formulae are again found in the paper by Mihalas and Stone (1968). The collisional ionization rate for the transition $n\ell \rightarrow \kappa$ is given by

$$C_{n\ell,\kappa} = CT^{1/2}\sigma_0[U_0E_1(U_0) - \frac{0.728}{U_1}E_1(U_1) - 0.189\,U_0^2e^{-U_0}\left(\frac{2+U_2}{U_2^3}\right) \quad , \quad (A2)$$

where $U_0 = E_{ion}/kT$, $U_1 = U_0 + 0.27$, $U_2 = U_0 + 1.43$ and σ_0 is a tabulated quantity given in the same paper.

Collisional Redistribution of Angular Momentum. For transitions with $\ell \leq 2$, the rates computed according to equation (A1) were used. Because an appreciable energy difference occurs between ℓ sublevels for $\ell \leq 2$, electrons are of dominant importance in the redistribution of angular momentum. However, for $\ell \geq 3$, the slower moving protons and the He$^+$ nuclei are more efficient than electrons in producing redistribution (Brocklehurst 1972). For $\ell \geq 3$, the formulation of Pengelly and Seaton (1964) was used to calculate the rate of redistribution of angular momentum.

Three Body Recombination. The three body recombination coefficients $\gamma_{n\ell}$ can be calculated from the equation of detail balance:

$$N_e^2 N_i \gamma_{n\ell} = N^*_{n\ell} N_e C_{n\ell,\kappa} \quad . \tag{A3}$$

Spontaneous Transition Probabilities. For transitions between levels with $\ell \leq 2$, the transition probabilities were calculated from the oscillator strengths given by Green, Johnson, and Kolchin (1966). For transitions with $\ell \geq 2$, the hydrogenic formula given by Brocklehurst (1971) was used:

$$A_{n\ell,n'\ell'} = 2.6774 \times 10^9 \; a_{n\ell,n'\ell'}$$

$$a_{n\ell,n'\ell'} = \left(\frac{1}{n'^2} - \frac{1}{n^2}\right) \frac{\max(\ell,\ell')}{(2\ell+1)} \left|\rho(n'\ell',n\ell)\right|^2 \quad . \tag{A4}$$

The squares of the radial matrix elements were computed using the method suggested by Gordon (1929). The Einstein coefficients for stimulated emission and absorption were calculated using the $A_{n\ell,n'\ell'}$.

Radiative Recombination. For $\ell < 2$, the radiative recombination rates were obtained from the paper by Burgess and Seaton (1960). For $\ell \geq 2$, the recombination rates were calculated using the formulae given by

Brocklehurst (1972).

Photoionization. For $\ell \geq 2$, formulas for the photoionization cross section are given by Brocklehurst (1971). For $\ell < 2$, the general formulation is necessary because of the nonhydrogenic character of the energy levels. From Burgess and Seaton (1959), if $I_{n\ell}$ is the threshold energy and E' is the energy of the ejected electron in Rydberg units, then

$$h\nu = I_{n\ell} + E'$$

and

$$a_{n\ell}(\nu) = 8.559 \times 10^{-19} \left(\frac{I_{n\ell} + E'}{I_{n\ell}^{2}}\right) \sum_{\ell' = \ell \pm 1} \frac{\max(\ell,\ell')}{2\ell + 1} \left|g(\bar{\nu},\ell;E',\ell')\right|^{2} , \tag{A5}$$

where $\bar{\nu}$ is the effective principal quantum number of the initial state and $g(\bar{\nu},\ell;E',\ell')$ is a quantity which must be calculated. Formulas for $g(\bar{\nu},\ell;E',\ell')$ are given in the same paper.